

# **A matrix isolation and computational study of molecular palladium fluorides: does PdF<sub>6</sub> exist?**

**Antony V. Wilson,<sup>†,#</sup> Timothy Nguyen,<sup>‡</sup> Felix Brosi,<sup>§</sup> Xuefeng Wang,<sup>¶,||</sup> Lester Andrews,<sup>¶</sup> Sebastian Riedel,<sup>§,⊥</sup> Adam J. Bridgeman,<sup>‡</sup> and Nigel A. Young<sup>\*†</sup>**

<sup>†</sup> Department of Chemistry, The University of Hull, Kingston upon Hull, HU6 7RX, U.K.

<sup>‡</sup> School of Chemistry, The University of Sydney, NSW 2006, Australia

<sup>§</sup> Institut für Chemie und Biochemie – Anorganische Chemie, Freie Universität Berlin, Fabeckstrasse 34-36, D-14195 Berlin, Germany

<sup>¶</sup> Department of Chemistry, University of Virginia, Charlottesville, Virginia, VA, 22904-4319, USA

<sup>⊥</sup> Institut für Anorganische und Analytische Chemie, Albert-Ludwigs-Universität Freiburg, Albertstrasse 21, D-79104 Freiburg im Breisgau, Germany

[\\*n.a.young@hull.ac.uk](mailto:n.a.young@hull.ac.uk)

44 1482 465442 (tel)

Current addresses

<sup>#</sup> Sungkyunkwan University, 2066 Seobu-Ro Jangan-Gu, Suwon-Si, Gyeonggi-Do 440-746, Korea

<sup>||</sup> Department of Chemistry, Tongji University, Shanghai, 200092, China.

## Abstract

Palladium atoms generated by thermal evaporation and laser ablation have been reacted with and trapped in  $F_2/Ar$ ,  $F_2/Ne$  and neat  $F_2$  matrices. The products have been characterized by electronic absorption and infrared spectroscopy, together with relativistic DFT calculations as well as coupled cluster calculations. Vibrational modes at 540 and 617  $cm^{-1}$  in argon matrices have been assigned to molecular PdF and PdF<sub>2</sub> and a band at 692  $cm^{-1}$  has been assigned to molecular PdF<sub>4</sub>. A band at 624  $cm^{-1}$  can be assigned to either PdF<sub>3</sub> or PdF<sub>6</sub>, with the former preferred from experimental considerations. Although calculations might support the latter assignment, our conclusion is that in these detailed experiments there is no convincing evidence for PdF<sub>6</sub>.

## Introduction

There has been considerable recent activity in understanding the limits of stability of the high oxidation states of 4d and 5d transition metal complexes.<sup>1,2</sup> In this context, the question of whether mercury should be regarded as a transition metal has been raised.<sup>3-6</sup> There is compelling experimental evidence for the 4d hexafluorides of Mo to Rh and the 5d hexafluorides of W to Pt,<sup>7,8</sup> as well as ReF<sub>7</sub>.<sup>9</sup> Computational investigations (DFT and state of the art coupled-cluster (CC)) have indicated the stability of Pd(VI) in PdF<sub>6</sub> (DFT,<sup>10-13</sup> CC<sup>12</sup>); Tc(VII) in TcF<sub>7</sub> (CC),<sup>14</sup> Ir(VII) in IrF<sub>7</sub> (CC),<sup>15</sup> and that Os(VII) and Os(VIII) might exist as OsF<sub>7</sub> and OsF<sub>8</sub> (CC).<sup>16</sup> However, calculations indicate that AuF<sub>6</sub> and AuF<sub>7</sub> are unlikely to be stable<sup>17</sup> (despite the reported preparation of AuF<sub>7</sub><sup>18, 19</sup>), and that platinum fluorides higher than PtF<sub>6</sub> are also unlikely to be stable.<sup>20, 21</sup> In addition, calculations indicate the stability of Rh(VIII) in RhO<sub>4</sub>,<sup>22</sup> Ir(VIII) in IrO<sub>4</sub>,<sup>23</sup> and even Ir(IX) in [IrO<sub>4</sub>]<sup>+</sup>.<sup>24-26</sup> There is a lone experimental report of the preparation of PdF<sub>6</sub>, but its identification rests on a single IR band at 711 cm<sup>-1</sup>,<sup>27, 28</sup> and this has been questioned on the basis of calculations.<sup>1, 10</sup> It is reported that the only “real” Os(VII) compound known experimentally is OsOF<sub>5</sub> and that when the published conditions for the synthesis of OsF<sub>7</sub> were repeated, only OsF<sub>6</sub> was obtained.<sup>29</sup> Although there is reported evidence for IrO<sub>4</sub> with Ir(VIII) in low temperature matrices,<sup>23</sup> there was no evidence for Rh(VIII) in analogous experiments.<sup>22</sup> In addition to being vital to understanding the limits of chemical stability, the more stable, high oxidation state fluorides can be used as potent oxidizers.<sup>30, 31</sup>

Of the “missing” hexafluorides,<sup>2</sup> PdF<sub>6</sub> is probably the most surprising, given that all the other 4d and 5d hexafluorides of Groups 6-8 are known,<sup>7, 8</sup> including PtF<sub>6</sub>,<sup>32, 33</sup> which was instrumental in the development of xenon chemistry as long ago as 1962.<sup>34, 35</sup> There appear to be no experimental reports on PdF. PdF<sub>2</sub> adopts the rutile structure in the solid state.<sup>36</sup> PdF<sub>3</sub> is mixed valence, containing Pd(II)[(Pd(IV)F<sub>6</sub>], with both palladium atoms in an octahedral environment.<sup>37-40</sup> PdF<sub>4</sub> is diamagnetic and has octahedral coordination in the solid state with two terminal *cis* F atoms and four bridging F atoms.<sup>41, 42</sup> It should be noted that whilst XeF<sub>2</sub> will oxidize PtF<sub>4</sub> and “PdF<sub>3</sub>”, it will not oxidize PdF<sub>4</sub>.<sup>39</sup> Apart from the single report on PdF<sub>6</sub><sup>27, 28</sup> there appears to be no other experimental data available for the molecular palladium fluorides, including PdF. However, there has been considerable computational activity in recent years because of the possibility of both Jahn-Teller and spin-orbit effects manifesting themselves.<sup>10-13, 43-47</sup>

Here we report an experimental and quantum-chemical investigation of the binary palladium fluorides from PdF to PdF<sub>6</sub>. Several matrix-isolation setups around the world (UK, USA and Germany)

have been involved in these experiments using both thermal evaporation and laser ablation to generate palladium atoms for reaction with F<sub>2</sub> doped Ar and Ne matrices as well as neat F<sub>2</sub> matrices. In addition quantum-chemical calculations utilising both relativistic DFT and coupled-cluster have been performed to characterize the species in question.

### Experimental and Computational Details

The matrix isolation equipment used for thermal evaporation<sup>48-50</sup> and laser ablation experiments<sup>51-53</sup> has been described in detail before. The thermal evaporation studies performed at the University of Hull used palladium wire (0.1 mm, 99.99% Goodfellow) wound around and within three strands of a tantalum wire hairpin former (0.5 mm, 99.99% Goodfellow) which was heated using *ca.* 40 A at 1 V. To avoid heating of the window and matrix deposit a copper disc with a 5 mm aperture was placed between the furnace and the vacuum chamber containing the deposition window. The F<sub>2</sub>/Ar mixtures were prepared using standard manometric procedures from 10% F<sub>2</sub>/Ar (Air Liquide) using an all metal vacuum line. The vacuum line, reservoirs and vacuum chamber were well passivated. The IR spectra were recorded using KBr beamsplitters and DTGS detectors on Bruker IFS66 and EquNox55 FTIR instruments equipped with APD DE-204 cryostats with base temperatures of *ca.* 10 K. The electronic absorption spectra were recorded on a Varian Cary 5E UV-vis-NIR spectrometer equipped with an APD DE-202 cryostat with a base temperature of *ca.* 12 K. Broadband photolysis ( $\lambda > 250$  nm) was carried with a LOT-Oriel 200 W Hg(Xe) lamp. The laser ablation investigations performed at the Universities of Freiburg/Berlin and Virginia employed Sumitomo 205 cryocoolers reaching 5 K second stage temperatures and Nicolet 750 (Virginia) or Bruker Vertex 70 (Freiburg/Berlin) FTIR spectrometers equipped with HgCdTe range B liquid nitrogen cooled detectors. The apparatus at Freiburg/Berlin is similar to that at Virginia, but there are differences in Freiburg/Berlin such as the magnetic rotating device for a fixed target, 25 mm of CsI window exposed to the laser ablation plume, and the lack of a radiation shield. The Virginia experiments with only 12.5 mm of cold window exposed from the OFHC copper mount and radiation shield, employed slightly higher ablation laser energies.

**Caution:** Fluorine is a powerful oxidizer and toxic. Suitable storage and handling facilities must be used, as well as shielding, protective clothing and face masks. Extensive care must be taken to avoid contact between fluorine, fluorides and oxidizable materials. An initial layer of argon should be used to protect the CsI deposition window when neat F<sub>2</sub> matrices are employed.

The simple valence force field calculations (SVFF) utilised SOTONVIB.<sup>54</sup> DFT calculations were performed using the ADF program,<sup>55-57</sup> at the BP86<sup>58-60</sup> level with triple- $\zeta$  (TZ2P) Slater-type orbital basis sets and relativistic effects at the ZORA level.<sup>61</sup> Spin-orbit coupling was included, as appropriate, in the structure optimizations and in analysis of the thermochemistry. Zero point and basis set supposition error corrections were also incorporated in the thermochemical analysis. Harmonic frequency calculations were performed at all optimized structures. Beyond the investigations using the ADF code we also performed DFT calculations using Gaussian09<sup>62</sup> and for coupled-cluster, the CFOUR program package.<sup>63</sup> Structure optimizations for all possible spin states were first performed using the B3LYP functional with the aug-cc-pVTZ basis set for fluorine and the aug-cc-pVTZ-PP basis set for Pd using the relativistic small core pseudopotential of the Stuttgart-Koeln type (MCDHF RSC ECP).<sup>64</sup> The most stable configuration was then used as the starting structure for the coupled-cluster calculations. Harmonic frequency calculations were performed at all optimized structures.

## Results

The key to interpreting the matrix IR data is (i) identifying the vibrational modes that involve Pd and F, (ii) determining the number of fluorine atoms coordinated to the Pd and (iii) confirming the molecular shape of the  $\text{PdF}_n$  species formed. Unfortunately, F is mono-isotopic so determining the PdF coordination number is not straight-forward from the vibrational data alone. However, Pd does have isotopes that are sufficiently well separated to give observable isotope patterns in well

resolved matrix IR data. Figure 1 displays a series of SVFF calculated Pd isotope patterns for the IR active  $\nu_{\text{Pd-F}}$  modes of different  $\text{PdF}_n$  species using the same transition wavenumber ( $^{106}\text{Pd}$  at  $633.0\text{ cm}^{-1}$ ) and bandwidth ( $0.5\text{ cm}^{-1}$  fwhm). Whilst it is clear that the pattern expected for PdF (and “PdF” units) is reasonably distinct from the others with a separation of *ca.*  $0.9\text{ cm}^{-1}$  between the  $^{106}\text{PdF}$  and  $^{108}\text{PdF}$  components, the calculated pattern for the other stoichiometries and geometries are more similar. The  $^{106}\text{PdF}$  and  $^{108}\text{PdF}$  separation is  $1.5\text{ cm}^{-1}$  for linear  $\text{PdF}_2$ ,  $1.25\text{ cm}^{-1}$  for  $120^\circ$  in  $\text{PdF}_3$  and  $1.15\text{ cm}^{-1}$  for  $109.47^\circ$  in tetrahedral  $\text{PdF}_4$ . The calculated IR Pd isotope patterns for  $\text{D}_{4h}$   $\text{PdF}_4$  and  $\text{O}_h$   $\text{PdF}_6$  are essentially identical to that of linear  $\text{PdF}_2$  as the  $\text{E}_u$  ( $\text{D}_{4h}$ ) and  $\text{T}_{1u}$  ( $\text{O}_h$ ) modes are essentially just orthogonal  $\text{PdF}_2$  asymmetric stretching modes. Likewise, the pattern for  $\text{D}_{3h}$   $\text{PdF}_3$  is essentially identical to that from  $\text{PdF}_2$  with a  $120^\circ$  bond angle, and that from  $\text{T}_d$   $\text{PdF}_4$  is the same as that for a  $\text{PdF}_2$  unit with a  $109.47^\circ$  bond angle. Therefore, these calculations show that PdF will give rise to a characteristic isotope pattern, but that the spectra of linear  $\text{PdF}_2$ , square planar  $\text{PdF}_4$  and octahedral  $\text{PdF}_6$  will be essentially identical in terms of both the number of bands expected, and the Pd isotope structure on them. Any deviation from linearity of the “PdF<sub>2</sub>” units will result in a reduced separation of the Pd isotopic features, but for slight distortions from linearity this will be fairly small due to the nature of the sine function. Therefore, whilst it will be possible to identify PdF modes belonging to  $\text{PdF}_n$  species from the characteristic palladium isotopic structure, it is anticipated that assignment of the IR features to individual compounds will be challenging and that insights from computational chemistry will be vital to obtaining a full assignment.

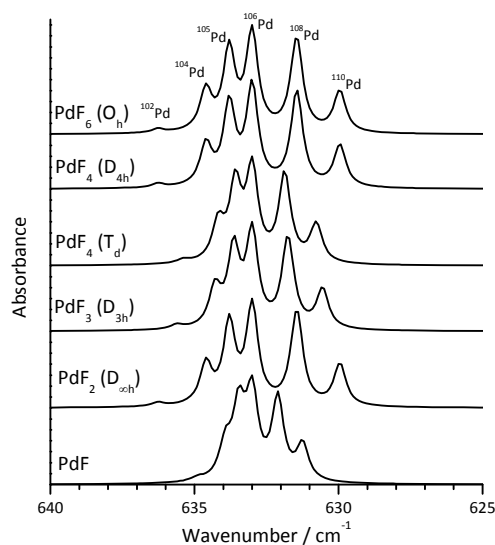


Figure 1. SVFF calculated palladium isotope patterns for IR active modes in a variety of prototypical geometries.

## Computational chemistry

Care needs to be exercised in order to get an accurate description of the palladium fluorides because of the possibility of considerable Jahn-Teller, spin-orbit and relativistic effects. Whilst there have been a number of computational reports on the palladium fluorides,<sup>10-13, 43-46, 65-68</sup> there is no systematic study of all possible PdF<sub>n</sub> species available in the literature. As it is anticipated that there will be a mixture of species formed, a detailed computational study of the ground state structures, spin states, vibrational data as well as selected thermochemical values was carried out for PdF<sub>n</sub> (n = 1 to 6) using both DFT and CCSD methods. As it has been shown previously that spin-orbit coupling needs to be included,<sup>11, 69</sup> we have concentrated on the results of our relativistic DFT calculations which include spin-orbit coupling, and the calculated ground state structures, electronic ground terms, and vibrational data for PdF<sub>n</sub> (n = 1 – 6) are given in Table 1. For PdF<sub>4</sub> and PdF<sub>6</sub> there is considerable debate about whether the structures are Jahn-Teller distorted, or subject to spin-orbit effects which quench this distortion, and whether the deviations from regular *D*<sub>4h</sub> and *O*<sub>h</sub> geometries would be detectable.<sup>10-12, 46, 69</sup> Our calculations using DFT and CCSD without spin-orbit coupling, together with a summary of earlier data<sup>10, 11, 13, 43, 44</sup> are given in the supplementary data. (There is one computational report that deals with many PdF<sub>n</sub> species.<sup>13</sup> However, no ground terms or vibrational energies are given, many of the geometries are different to previous calculations and the electronic configuration of Pd is reported as [Kr]4d<sup>10</sup>5s<sup>1</sup>, therefore we have not included these results in our discussion.)

**Table 1** Summary of relativistic DFT computational results<sup>a</sup>

			Pd-F /Å	F-Pd-F /°	v <sub>Pd-F</sub> modes / cm <sup>-1</sup> (symmetry species, IR intensity)
PdF	<i>C</i> <sub>∞v</sub>	<sup>2</sup> Σ <sup>+</sup>	1.930		533.9 (Σ <sup>+</sup> , 41)
PdF <sub>2</sub>	<i>D</i> <sub>∞h</sub>	<sup>3</sup> Π <sub>g</sub>	1.895	180	633.5 (Σ <sub>u</sub> <sup>+</sup> , 146), 560.9 (Σ <sub>g</sub> <sup>+</sup> , 0)
PdF <sub>3</sub>	<i>C</i> <sub>2v</sub>	<sup>2</sup> A <sub>2</sub>	1.865 (x2) 1.886	168.0 96.0	661.8 (B <sub>2</sub> , 117), 591.9 (A <sub>1</sub> , 0.86), 565.3 (A <sub>1</sub> , 39.7)
PdF <sub>4</sub>	<i>D</i> <sub>4h</sub>	A <sub>1</sub> ( <sup>3</sup> E <sub>g</sub> )	1.866	90	663.5 (E <sub>u</sub> , 81.6 x 2), 585.6 (A <sub>1g</sub> , 0), 523.7 (B <sub>1g</sub> , 0)
PdF <sub>5</sub>	<i>C</i> <sub>4v</sub>	<sup>2</sup> B <sub>2</sub>	1.878 (x4) 1.854	173.03 93.5, 89.8	648.3 (E, 79.1 x 2), 632.7 (A <sub>1</sub> , 15.5), 578.6 (A <sub>1</sub> , 0.95), 552.6 (B <sub>1</sub> , 0)
PdF <sub>6</sub>	<i>O</i> <sub>h</sub>	A <sub>1</sub> ( <sup>3</sup> T <sub>1g</sub> )	1.876	180, 90	648.0 (T <sub>1u</sub> , 58.7 x 3), 574.0 (A <sub>1g</sub> , 0), 541.2 (E <sub>g</sub> , 0 x 2)

<sup>a</sup> ADF, BP86, TZ2P, ZORA.

**PdF** is predicted to have a <sup>2</sup>Σ<sup>+</sup> ground state, in agreement with Schwerdtfeger,<sup>65</sup> Siegbahn<sup>43</sup> and Cheng.<sup>45</sup> Our calculated Pd-F distance is 1.930 Å compared to 2.01 Å from Siegbahn<sup>43</sup> and 1.961 Å

from Cheng.<sup>45</sup> The harmonic frequency of  $533.9\text{ cm}^{-1}$  is very similar to that of  $531\text{ cm}^{-1}$  calculated by Cheng.<sup>45</sup>

**PdF<sub>2</sub>** is calculated to have a linear,  ${}^3\Pi_g$  ground state, based on a  $(\delta_g)^4(\pi_g)^3(\sigma_g)^1$  ligand-field occupation, with the IR active  $\Sigma_g^+$   $\nu_{\text{PdF}}$  mode at  $633.5\text{ cm}^{-1}$ . The  ${}^3\Sigma_g^+$  state was calculated to lie *ca.*  $20\text{ kJ mol}^{-1}$  higher than the  ${}^3\Pi_g$  ground state. The lowest energy singlet is found to be strongly bent, with a bond angle of  $102^\circ$ , and *ca.*  $40\text{ kJ mol}^{-1}$  higher than the  ${}^3\Pi_g$  ground state. The lowest energy linear singlet state is *ca.*  $50\text{ kJ mol}^{-1}$  higher in energy. Siegbahn also predicted a  ${}^3\Pi_g$  ground state for PdF<sub>2</sub>.<sup>44</sup> The PdF<sub>2</sub> bond length is calculated to be  $1.895\text{ \AA}$ , compared to  $1.94\text{ \AA}$  from Siegbahn.<sup>44</sup> In contrast, Wesendrup and Schwerdtfeger<sup>20</sup> found a linear, triplet  ${}^3\Sigma_g^+$  ground state for PtF<sub>2</sub>, based on the ligand-field occupation  $(\delta_g)^4(\sigma_g)^2(\pi_g)^2$ .

**PdF<sub>3</sub>** is calculated to have a spin-doublet ( ${}^2A_2$ ) T-shaped structure with one longer ( $1.886\text{ \AA}$ ) and two slightly shorter ( $1.865\text{ \AA}$ ) Pd-F bonds. The IR active  $\nu_{\text{PdF}}$  modes are predicted to be at  $661.8\text{ cm}^{-1}$  ( $B_2$ ),  $591.9\text{ cm}^{-1}$  ( $A_1$ ) and  $565.3\text{ cm}^{-1}$  ( $A_1$ ) with an intensity ratio of 136:1:46. A recent theoretical report on XePdF<sub>3</sub> has indicated a 'T'-shaped structure with  $C_1$  point group for PdF<sub>3</sub>, but no bond lengths or angles were given.<sup>68</sup> This work also highlighted the challenge these type of molecules present to computational chemistry.

**PdF<sub>4</sub>** Optimization of the ground state of PdF<sub>4</sub> leads to a very slightly distorted square planar molecule based on a Jahn-Teller distortion of the  ${}^3E_g$  state. The  $D_{2d}$  geometry is very slightly non-planar with bond angles which alternate by less than  $0.5^\circ$  in keeping with the results obtained by Aullón and Alvarez for PdF<sub>4</sub><sup>10</sup> and for PtF<sub>4</sub> by Wesendrup and Schwerdtfeger.<sup>20</sup> However, when spin-orbit coupling is included, even this small distortion is quenched, yielding a  $D_{4h}$  structure with an  $A_1$  ground state,  $1.866\text{ \AA}$  bond lengths and a single IR active  $\nu_{\text{PdF}}$  mode at  $663.5\text{ cm}^{-1}$ . Fig. 2 shows the effect of spin-orbit coupling on the *d*-orbitals with loss of the orbital degeneracy responsible for the Jahn-Teller activity. This observation is in keeping with that of David *et al.* for the hexafluorides.<sup>11, 69, 70</sup> Our CCSD calculations without spin-orbit coupling retain a planar, distorted  $D_{2h}$

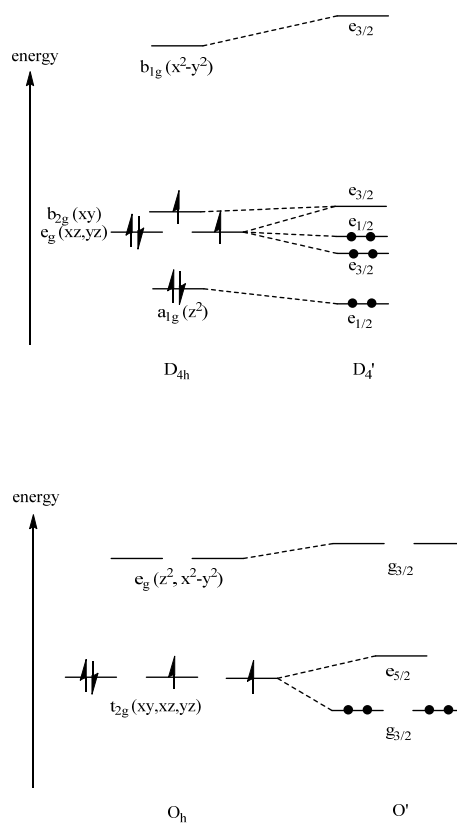


Figure 2. Effect of spin-orbit coupling on the *d* orbitals of PdF<sub>4</sub> (top) and PdF<sub>6</sub> (bottom).

structure with 1.805 and 1.848 Å Pd-F distances. These CCSD calculations indicate that there will be two IR active  $\nu_{\text{PdF}}$  modes, at 750.4 and 707.7  $\text{cm}^{-1}$ .

**PdF<sub>5</sub>** is calculated at the relativistic DFT level to have a square-pyramidal ( $C_{4v}$  symmetry)  ${}^2B_2$  ground state with an almost square base and with the axial Pd-F bond slightly shorter (1.854 Å) than the equatorial Pd-F bonds (1.878 Å), with one intense IR band at 648.3  $\text{cm}^{-1}$ , together with a weak feature at 632.7  $\text{cm}^{-1}$  and a very very weak feature at 578.6  $\text{cm}^{-1}$ . The CCSD calculations also yielded a  $C_{4v}$  structure, with identical axial and equatorial distances (1.836 Å).

**PdF<sub>6</sub>** behaves in a similar way to PdF<sub>4</sub>. In the absence of spin-orbit coupling, the  ${}^3T_{1g}$  ground state of octahedral PdF<sub>6</sub>, based on the expected low-spin ( $t_{2g}$ )<sup>4</sup> ligand-field configuration, undergoes a very small Jahn-Teller distortion to give a  $D_{4h}$  minimum, in keeping with the calculations of Aullón and Alvarez<sup>10</sup> for PdF<sub>6</sub> and Wesendrup and Schwerdtfeger<sup>20</sup> for PtF<sub>6</sub>. The inclusion of spin-orbit coupling quenches the distortion so that PdF<sub>6</sub> is predicted to be fully octahedral with an  $A_1$  ground state, a Pd-F bond length of 1.876 Å and the IR active  $\nu_{\text{Pd-F}}$  mode at 648.0  $\text{cm}^{-1}$ . This result is consistent with the LDA calculations of David *et al.* on PdF<sub>6</sub><sup>11</sup> and the Group 11 hexafluoride anions.<sup>69</sup> Alvarez-Thon *et al.* have commented that prior to 2008 all of the published non-relativistic and scalar relativistic calculations had predicted that PtF<sub>6</sub> was a paramagnetic distorted octahedral molecule with a triplet ground state, and that the four component spin-free method also predicted a distorted octahedral molecule with axial distortion due to a Jahn-Teller distortion.<sup>70</sup> However, a diamagnetic, octahedral singlet molecule was predicted when a four component Dirac molecular Hartree-Fock, DFT and two component zeroth-order regular approach (ZORA) methodology was employed. They concluded that the calculated octahedral molecular structure, in agreement with the NMR and vibrational spectroscopic data, was stabilized by the effect of spin-orbit coupling.

Figure 2 illustrates how spin-orbit coupling leads to the loss in the orbital degeneracy in this system. Our CCSD calculations (without spin-orbit coupling) result in a  $D_{4h}$  structure with Pd-F of 1.827 and 1.841 Å, and two IR active  $\nu_{\text{PdF}}$  modes at 724.5 and 718.0  $\text{cm}^{-1}$ . Craciun *et al.*<sup>12</sup> predicted that at the CCSD(T)/CBS level the ground state of PdF<sub>6</sub> would be  $D_{4h}$  with a  ${}^3A_{1g}$  term, but that the  $O_h$  structure was within 2  $\text{kJ mol}^{-1}$  of this ground state structure. Their BLYP/TZ2P ZORA – spin orbit calculations predicted that the  $D_{3d}$  structure was more stable by 0.5  $\text{kJ mol}^{-1}$ . A  ${}^1A_{1g}$  state was found to be *ca.* 50  $\text{kJ mol}^{-1}$  higher in energy than these triplet states. An average Pd-F distance of 1.849 Å was obtained from the CCSD(T) calculations for the  $D_{4h}$  structure, compared to an average of *ca.* 1.91 Å from the BLYP ZORA spin-orbit calculations. The IR active  $\nu_{\text{PdF}}$  modes were calculated at the B3LYP/ATZ-PP level to be 692 and 671  $\text{cm}^{-1}$ .<sup>12</sup> They concluded that because the  $D_{4h}$ ,  $D_{3d}$  and  $O_h$  structures were very close in energy, the 4d MF<sub>6</sub> molecules would be highly fluxional and exhibit an average  $O_h$  geometry

under most experimental conditions. They also noted that unlike the 5d hexafluorides, the inclusion of spin-orbit effects was unimportant to account for the ordering of the electron affinities. Aullón and Alvarez calculated the B3LYP Pd-F<sub>eq</sub> and Pd-F<sub>ax</sub> bond lengths to be 1.894 Å and 1.890 Å, with IR active Pd-F stretching modes at 585 and 530 cm<sup>-1</sup>.<sup>10</sup>

The relativistic DFT calculated vibrational data is in Table 1 and Fig. 3 displays the calculated IR spectra to aid with the spectral assignments (the isotopic data has been omitted for clarity). From these data it is expected that PdF, PdF<sub>2</sub>, PdF<sub>4</sub> and PdF<sub>6</sub> will all display one IR active Pd-F stretching mode, and from the previous discussion the last three will have essentially identical Pd isotope patterns. The calculations also indicate that the most intense ν<sub>Pd-F</sub> modes will be in the wavenumber order PdF<sub>4</sub> ≈ PdF<sub>3</sub> > PdF<sub>6</sub> ≈ PdF<sub>5</sub> > PdF<sub>2</sub> >> PdF. (Our CC calculations also indicate that the IR active vibrational mode of PdF<sub>4</sub> will be at higher wavenumber than PdF<sub>6</sub>.) For PdF<sub>3</sub> two bands are expected, separated by about 100 cm<sup>-1</sup>, with the higher one significantly more intense than the lower one (approximately 3:1). The more intense B<sub>2</sub> mode is expected to have a similar isotope pattern to that of PdF<sub>2</sub> as it is the asymmetric stretch of the bar in the 'T'-shaped molecule. The lower energy A<sub>1</sub> mode with some IR intensity is predominantly the symmetric stretch of the handle of the 'T'-shaped molecule so will have a Pd isotope pattern more characteristic of a "PdF" unit. Square

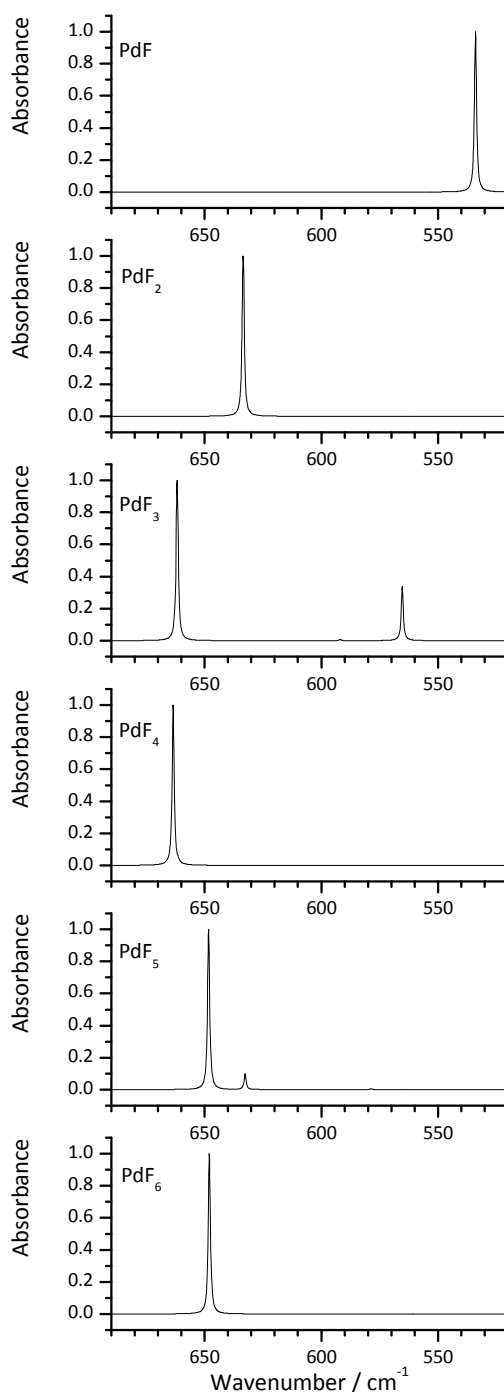


Figure 3. Relativistic DFT calculated IR spectra for PdF<sub>n</sub> species (ignoring Pd isotopes)

pyramidal PdF<sub>5</sub> is predicted to have one intense IR active  $\nu_{\text{Pd-F}}$  E mode with a characteristic “PdF<sub>2</sub>” isotope pattern, with a weaker A<sub>1</sub> (predominantly axial  $\nu_{\text{Pd-F}}$ ) mode which may not be detectable above the noise limit. In this case, the separation of the Pd isotope features is slightly larger than that for predicted “PdF<sub>2</sub>” and “PdF” units, 1.58 vs. 1.50 cm<sup>-1</sup> and 1.01 vs. 0.90 cm<sup>-1</sup>, but this is very much at the margins of experimental detection.

Therefore, the principal IR active  $\nu_{\text{Pd-F}}$  modes for all of the possible PdF<sub>n</sub> species apart from PdF are predicted to have very similar Pd isotope patterns. To complicate matters further, the calculations indicate that the IR active  $\nu_{\text{Pd-F}}$  modes in PdF<sub>3</sub> and PdF<sub>4</sub> will overlap, as will those of PdF<sub>5</sub> and PdF<sub>6</sub>, but that the PdF and PdF<sub>2</sub>  $\nu_{\text{Pd-F}}$  modes will be distinct. Aullón and Alvarez calculated that the IR active  $\nu_{\text{Pd-F}}$  modes in PdF<sub>4</sub> and PdF<sub>6</sub> would overlap as well.<sup>10</sup> As noted previously, the published calculated Pd-F stretching modes for PdF<sub>6</sub> range from 585 to 725 cm<sup>-1</sup>. Hence, an unambiguous assignment will be challenging. However, the fluorine concentration in these experiments will help to identify the higher valent fluorine species as it is expected that a higher concentration of fluorine will favour the higher valent palladium fluorides.

The relativistic DFT thermochemical data is collected together in Table 2, and this shows that the formation of all of the PdF<sub>n</sub> (n = 1 - 6) species is thermodynamically favourable. We have concentrated on the enthalpy terms on the assumption that the entropy contributions will be small due to the low temperature of experiment.

In addition, calculating entropy and hence free energy relationships for matrix isolated species is non-trivial due to the quenching of the rotational and translational entropy components. The calculation of the F<sub>2</sub> bond enthalpy by DFT methods is notoriously challenging,<sup>71</sup> but this only affects the absolute, rather than relative values of the PdF<sub>x</sub> thermochemical data.

Due to the F<sub>2</sub> dilution used in the matrix experiments it is expected that a range of species will be formed, and it is illustrative to use the stepwise thermochemistry to investigate the likelihood of formation of the species sequentially, and these are presented in Table 2 and graphically in Figure 4. These demonstrate that whilst all the PdF<sub>n-1</sub> + ½F<sub>2</sub> → PdF<sub>n</sub> reactions are thermodynamically favourable, they become progressively less exothermic on going from PdF<sub>2</sub> to the higher

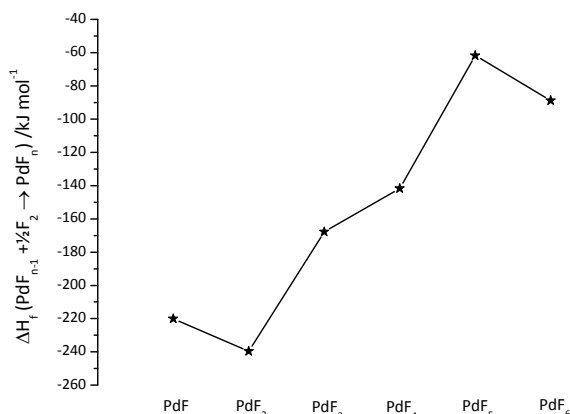


Figure 4. Stepwise formation enthalpies of palladium fluorides

coordination numbers. It should also be noted that if fluorine atoms are present, the reactions will become much more favourable. The photolysis of  $F_2$  in cryogenic matrices not only results in fluorine atoms, but that these fluorine atoms are able to travel considerable distances beyond the immediate cage where they are formed.<sup>72-74</sup> Table 2 and Fig. 4 also highlight that  $PdF_5$  is unstable with respect to disproportionation to  $PdF_6$  and  $PdF_4$ , and whilst the disproportionation of  $PdF_3$  is predicted to be slightly endothermic ( $26 \text{ kJ mol}^{-1}$ ), it is still relatively favourable at the DFT level. Whilst disproportionation of mononuclear complexes is not expected in dilute matrices, it gives some idea of the stability of the products formed. Therefore, the conclusion based on relativistic DFT level thermochemistry is that the most stable species are  $PdF$ ,  $PdF_2$ ,  $PdF_4$  and  $PdF_6$ , followed by  $PdF_3$  and then  $PdF_5$ .

Table 2. Summary of thermochemistry from relativistic DFT calculations<sup>a</sup>

Overall $\Delta H_f$	$\text{kJ mol}^{-1}$	Stepwise $\Delta H_f$	$\text{kJ mol}^{-1}$	$\Delta H$ for selected reactions	$\text{kJ mol}^{-1}$
$Pd + \frac{1}{2} F_2 \rightarrow PdF$	-220	$Pd + \frac{1}{2} F_2 \rightarrow PdF$	-220	$2PdF \leftrightarrow PdF_2 + Pd$	-20
$Pd + F_2 \rightarrow PdF_2$	-460	$PdF + \frac{1}{2} F_2 \rightarrow PdF_2$	-240	$2PdF_2 \leftrightarrow PdF_4 + Pd$	150
$Pd + 3/2 F_2 \rightarrow PdF_3$	-627	$PdF_2 + \frac{1}{2} F_2 \rightarrow PdF_3$	-167	$2PdF_2 \leftrightarrow PdF_3 + PdF$	72
$Pd + 2F_2 \rightarrow PdF_4$	-769	$PdF_3 + \frac{1}{2} F_2 \rightarrow PdF_4$	-142	$2PdF_3 \leftrightarrow PdF_6 + Pd$	335
$Pd + 5/2 F_2 \rightarrow PdF_5$	-831	$PdF_4 + \frac{1}{2} F_2 \rightarrow PdF_5$	-62	$2PdF_3 \leftrightarrow PdF_4 + PdF_2$	26
$Pd + 3F_2 \rightarrow PdF_6$	-920	$PdF_5 + \frac{1}{2} F_2 \rightarrow PdF_6$	-89	$2PdF_4 \leftrightarrow PdF_6 + PdF_2$	159
				$2PdF_5 \leftrightarrow PdF_6 + PdF_4$	-27
				$PdF_5 + Pd \leftrightarrow PdF_3 + PdF_2$	-256
				$PdF_5 + Pd \leftrightarrow PdF_4 + PdF$	-158
				$3PdF \leftrightarrow PdF_3 + 2Pd$	33
				$5PdF \leftrightarrow 2PdF_2 + 3Pd + F$	181

<sup>a</sup> ADF, BP86, TZ2P, ZORA

## Thermal evaporation experiments

### Electronic Absorption Spectra

Initially, electronic absorption spectroscopy was used to confirm the presence of Pd atoms within the matrix using the thermal evaporation source. Historically, the assignment of the correct features to Pd atoms took time to resolve as it is very easy to form Pd(N<sub>2</sub>) and Pd(N<sub>2</sub>)<sub>2</sub> even in the absence of a vacuum leak due to nitrogen adsorption onto the Pd filament.<sup>75-83</sup> It should also be noted that as Pd atoms have a 4d<sup>10</sup> ground state configuration, the propensity for dimer formation is small, and the intensity of any dimer bands very weak.<sup>77</sup> Figure 5(a)

confirms the presence of Pd atoms in 1% F<sub>2</sub>/Ar matrices when thermal evaporation was used. Apart from the shoulder at 46920 cm<sup>-1</sup>, the spectral features at 40310, 42300, 45410 cm<sup>-1</sup> are essentially identical to those of Pd atoms in argon matrices.<sup>75-82</sup> On annealing to 18 K the Pd atomic spectral features were replaced by broader ones at 40210, 45880 and 49010 cm<sup>-1</sup>. No further change was observed after broadband photolysis (Fig 5(c)). The very weak features in the 1%F<sub>2</sub>/Ar spectra at ca. 30000 cm<sup>-1</sup> are most likely to be due to palladium dinitrogen species.<sup>79, 81</sup> When a 10% F<sub>2</sub>/Ar matrix was used, a broad peak at 38250 cm<sup>-1</sup> was observed on deposition in addition to the broader Pd atomic spectral features at 40200, 42350 and 45870 cm<sup>-1</sup> (Fig. 5(d)). The 38250 cm<sup>-1</sup> peak is not due to F<sub>2</sub> as this is observed as the weak,

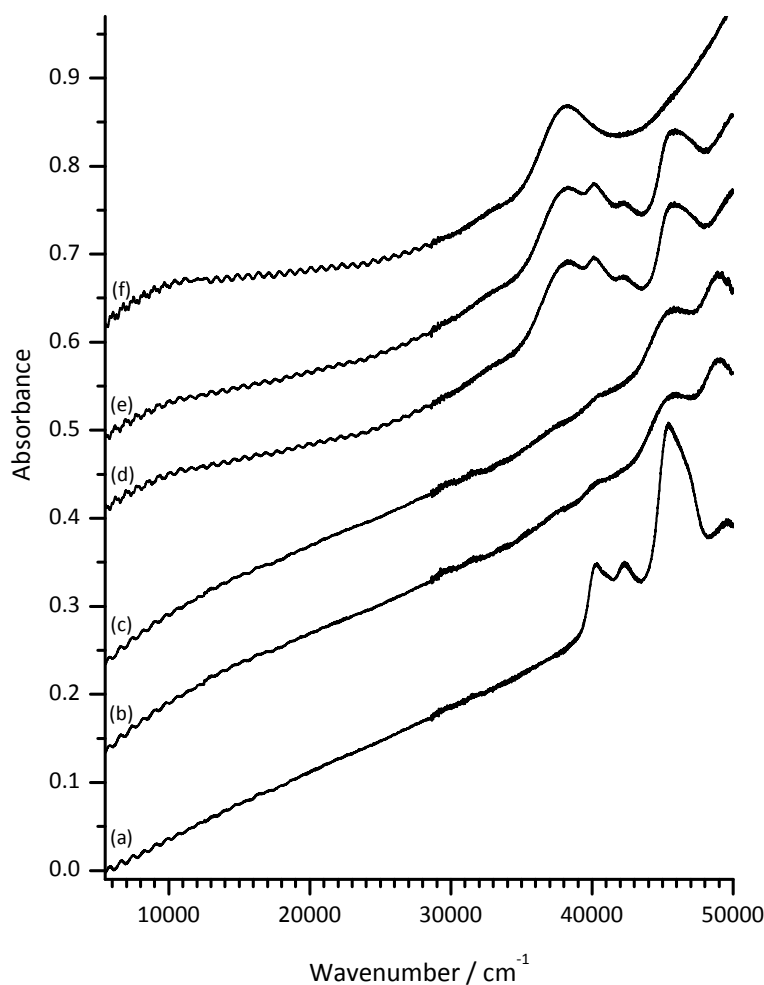


Figure 5. Electronic absorption spectra of Pd atoms and reaction products (a) in 1% F<sub>2</sub>/Ar matrix after deposition, (b) after annealing to 18 K, (c) after broadband photolysis, (d) in 10% F<sub>2</sub>/Ar matrix after deposition, (e) after broadband photolysis, (f) after annealing to 18 K.

features at 40310, 42300, 45410 cm<sup>-1</sup> are essentially identical to those of Pd atoms in argon matrices.<sup>75-82</sup> On annealing to 18 K the Pd atomic spectral features were replaced by broader ones at 40210, 45880 and 49010 cm<sup>-1</sup>. No further change was observed after broadband photolysis (Fig 5(c)). The very weak features in the 1%F<sub>2</sub>/Ar spectra at ca. 30000 cm<sup>-1</sup> are most likely to be due to palladium dinitrogen species.<sup>79, 81</sup> When a 10% F<sub>2</sub>/Ar matrix was used, a broad peak at 38250 cm<sup>-1</sup> was observed on deposition in addition to the broader Pd atomic spectral features at 40200, 42350 and 45870 cm<sup>-1</sup> (Fig. 5(d)). The 38250 cm<sup>-1</sup> peak is not due to F<sub>2</sub> as this is observed as the weak,

broad feature at  $35200\text{ cm}^{-1}$ .<sup>5</sup> On broadband photolysis (Fig. 5(e)) no difference was observed, but on annealing to 18 K (Fig. 5(f)), the atomic Pd features disappeared, to just leave the broad  $38250\text{ cm}^{-1}$  peak. In both sets of spectra there is also a weak and very broad band at low energy that is only observed when the products bands are present. Therefore, these experiments confirm that atomic Pd is being isolated in the thermal evaporation experiments and also indicate that there are at least two different species formed after annealing which are dependent on the  $\text{F}_2$  concentration, with photolysis having little effect in this case either before or after annealing.

## IR spectroscopy

A large number of experiments were carried out with a variety of matrix dilution ratios using fluorine doped argon and neon matrices, as well as neat fluorine matrices. In addition, both thermal evaporation and laser ablation techniques were used to generate palladium atoms, thus allowing for a comparison of the two methods. As in the case of the electronic absorption spectra, very weak bands arising from the  $\nu_{NN}$  modes of Pd(N<sub>2</sub>) and Pd(N<sub>2</sub>)<sub>2</sub> complexes,<sup>84, 85, 86</sup> as well as  $\nu_{OO}$  modes of Pd(O<sub>2</sub>),<sup>86, 87</sup> but not for (O<sub>2</sub>)Pd(N<sub>2</sub>)<sup>86, 88</sup> were observed in the IR spectra. These species arise from the reaction of palladium atoms with residual N<sub>2</sub> and O<sub>2</sub> in the matrix gases and the vacuum chambers and are a good indication that the experimental conditions have been optimized for palladium atom matrix reactions.

### Thermal evaporation experiments

When Pd atoms generated thermally from a Pd/Ta filament were condensed in a 2% F<sub>2</sub>/Ar matrix a number of bands were observed in the  $\nu_{Pd-F}$  region as shown in the survey spectrum (2cm<sup>-1</sup> resolution) in Fig. 6(a). (Those at 667 and 662 cm<sup>-1</sup> are due to gas phase and matrix isolated CO<sub>2</sub>, respectively.) On broadband photolysis (Fig.6(b)) the most marked differences are a reduction in intensity of the bands at 534 cm<sup>-1</sup> (**A**) and 624 cm<sup>-1</sup> (**D**), and an increase in the bands at 656 cm<sup>-1</sup> and 692 cm<sup>-1</sup> (**E**), together with a slight change in the band at 617 cm<sup>-1</sup> (**C**). On annealing to 20 K, there is a further increase in the band at 692 cm<sup>-1</sup> (**E**). The intense peak at 540 cm<sup>-1</sup> (**B**) remains invariant, whilst that at 617 cm<sup>-1</sup> (**C**) remains largely unaffected by either photolysis or annealing.

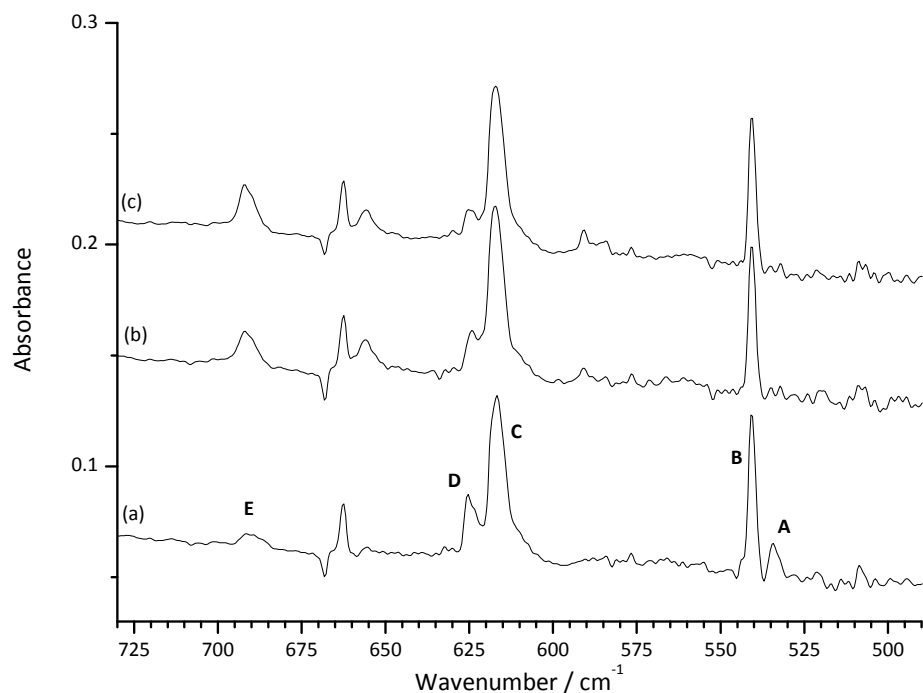


Figure 6. IR spectra ( $2\text{ cm}^{-1}$  resolution) of reaction products from thermally evaporated Pd atoms in a  $2\%$   $\text{F}_2/\text{Ar}$  matrix (a) on deposition, (b) after broadband photolysis, (c) after annealing to  $20\text{ K}$ .

At higher spectral resolution Pd isotope structure was observed on the bands labelled (A) – (E) in Fig. 6, and this is shown in more detail in the higher resolution ( $0.5\text{ cm}^{-1}$ ) spectrum obtained when Pd atoms generated from a Pd/Ta filament were condensed in a  $0.5\%$   $\text{F}_2/\text{Ar}$  matrix (Fig. 7(a)). Peaks with Pd isotopic fine structure were observed centred at  $624\text{ cm}^{-1}$  (D),  $617\text{ cm}^{-1}$  (C),  $540\text{ cm}^{-1}$  (B) and  $534\text{ cm}^{-1}$  (A). There was also a weak broad feature potentially with Pd isotopic fine structure at  $692\text{ cm}^{-1}$  (E). After Hg-Xe broadband photolysis (Fig. 7(b)), the initially very weak peak at  $692\text{ cm}^{-1}$  (E) grew in intensity and this confirmed the presence of Pd isotopic structure on this band. Its relative intensity compared to the  $617\text{ cm}^{-1}$  bands was less in the  $0.5\%$   $\text{F}_2/\text{Ar}$  matrix than in the  $2\%$   $\text{F}_2/\text{Ar}$  experiment. The effect of photolysis is shown more clearly in the difference spectra at the bottom of Fig. 7. Although a new feature at  $591\text{ cm}^{-1}$  also grew in on broadband photolysis in both the  $0.5\%$  and  $2\%$   $\text{F}_2/\text{Ar}$  experiments, on careful analysis it was shown that this does not possess Pd isotopic structure as it is made up of two bands that display different behaviour on annealing and photolysis. A new peak at  $656\text{ cm}^{-1}$  also appeared in both experiments, which whilst this displayed some structure, this was not consistent with a vibrational mode involving Pd. This peak was also observed in matrices with considerable  $\text{CO}_2$  features together with a peak at  $2356\text{ cm}^{-1}$  characteristic of  $\text{HF-CO}_2$ ,<sup>89</sup> and

with no other peaks displaying Pd isotope structure. Therefore, the peak at  $656\text{ cm}^{-1}$  is assigned to the HF-CO<sub>2</sub> complex,<sup>89</sup> rather than a PdF<sub>n</sub> complex. The peaks (**D**) centred at  $624\text{ cm}^{-1}$  reduced in intensity slightly on photolysis, and the structure on peak **C** at  $617\text{ cm}^{-1}$  changed slightly, and the intensity of some weak peaks on the low energy side of the **C** peaks reduced. Whilst there was no significant change in peak **B** at  $540\text{ cm}^{-1}$  the feature at  $534\text{ cm}^{-1}$  (**A**) all but disappeared on photolysis. (The peak at  $667\text{ cm}^{-1}$  is the Q-branch of the  $\nu_2$  mode of atmospheric CO<sub>2</sub>, there is also evidence of the P and R branch structures. These are due to small variations in the atmospheric CO<sub>2</sub> levels between background and sample spectra, and become more marked at higher resolution). After annealing to 25 K (Fig. 7(c)), the (**E**) peaks containing Pd isotope structure at  $692\text{ cm}^{-1}$  grew, those labelled (**B**) at  $540\text{ cm}^{-1}$  reduced in intensity slightly whilst those at  $534\text{ cm}^{-1}$  (**A**) completely disappeared. The (**D**) peaks at  $624\text{ cm}^{-1}$  all but disappeared and the structure within the **C** peaks at  $617\text{ cm}^{-1}$  again changed slightly, and weak peaks at slightly lower wavenumber than  $617\text{ cm}^{-1}$  grew in intensity. Whilst the peaks at both  $624\text{ cm}^{-1}$  (**D**) and  $534\text{ cm}^{-1}$  (**A**) reduced in intensity after broadband photolysis, this was not to the same extent and the subsequent annealing behaviour confirms that they do not belong to the same species. The peaks that show the most marked increase on photolysis are those labelled (**E**) at  $692\text{ cm}^{-1}$ , on annealing to 25 K these increase slightly again, accompanied by a more significant increase in those to the low energy side of the peaks at  $617\text{ cm}^{-1}$  (**C**). The behaviour of the (**E**) peaks on photolysis and annealing is not correlated with any of the other peaks bearing Pd isotopic structure.

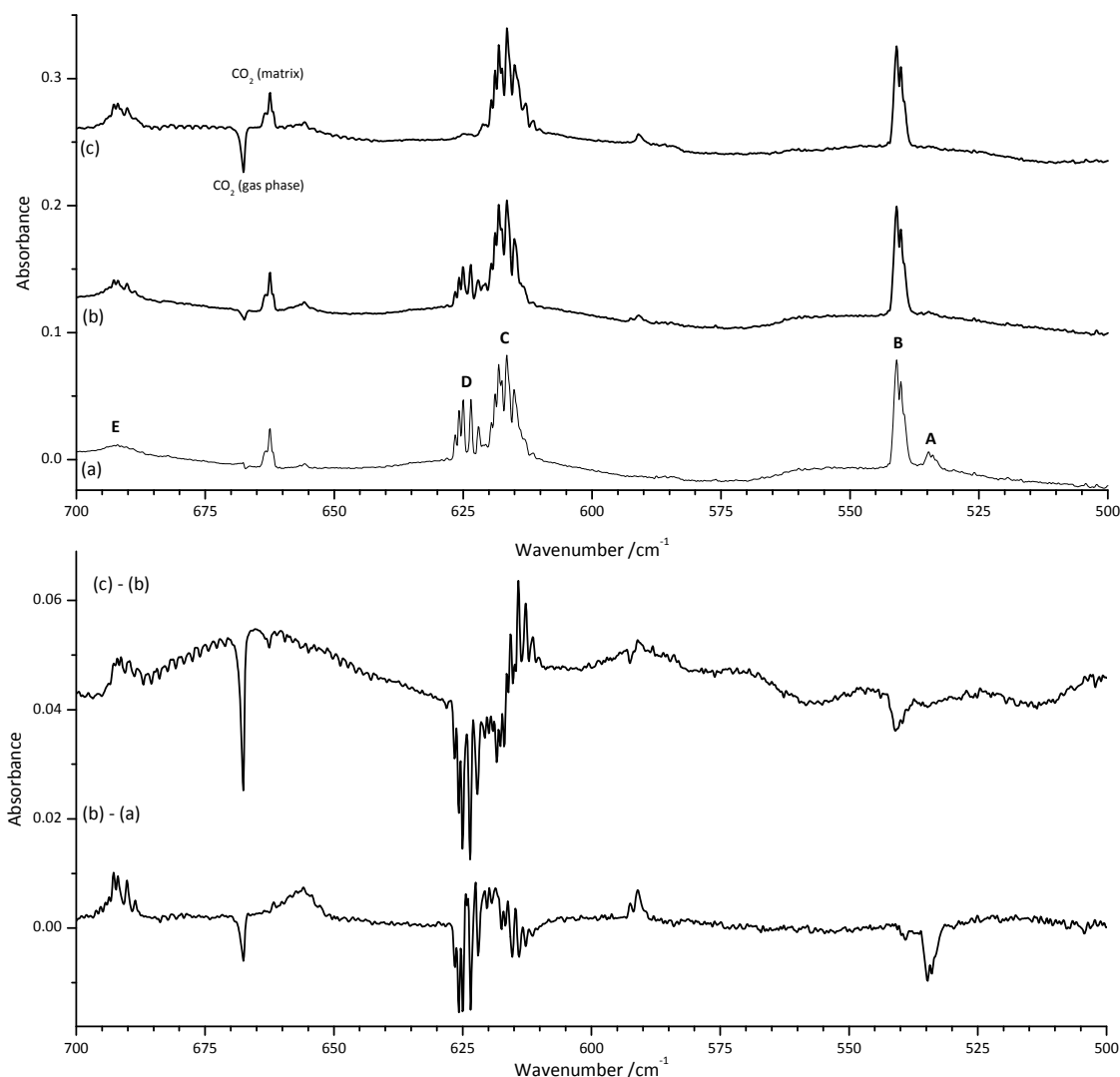


Figure 7. IR absorption (top) and difference (bottom) spectra ( $0.5 \text{ cm}^{-1}$  resolution) of reaction products from thermally evaporated Pd atoms in a  $0.5\% \text{ F}_2/\text{Ar}$  matrix (offset for clarity) (a) on deposition, (b) after Hg-Xe broadband photolysis, (c) after annealing to 25 K.

In a second experiment with a  $0.5\% \text{ F}_2/\text{Ar}$  matrix, the peaks labelled (**D**) at  $624 \text{ cm}^{-1}$  were relatively more intense than the (**C**) peaks at  $617 \text{ cm}^{-1}$ , and no (**A**) peak was observed at  $534 \text{ cm}^{-1}$ . This behaviour confirms that none of these bands are from the same species. On prolonged broad band photolysis in this second experiment, the  $624 \text{ cm}^{-1}$  (**D**) peaks were completely photobleached, before annealing. The peaks at  $692 \text{ cm}^{-1}$  (**E**),  $617 \text{ cm}^{-1}$  (**C**) and  $540 \text{ cm}^{-1}$  (**B**) behaved in the same way on photolysis and annealing as in the first experiment, except that the  $692 \text{ cm}^{-1}$  (**E**) peak was not as intense. In this experiment, the weak peaks on the low energy side of the **C** peaks grew on prolonged

broadband photolysis, but then reduced on annealing to 25 K, which is a reversal in behaviour to the experiment above. The peak at  $656\text{ cm}^{-1}$  again displayed no palladium isotope structure.

Therefore, from the survey spectra (Fig. 6 and Fig.7) it is clear that there are peaks centred at  $692\text{ cm}^{-1}$  (E),  $624\text{ cm}^{-1}$  (D),  $617\text{ cm}^{-1}$  (C),  $540\text{ cm}^{-1}$  (B) and  $534\text{ (A) cm}^{-1}$  which all display Pd isotopic structure. In addition the photolysis and annealing behaviour indicates that they each arise from distinct  $\text{PdF}_n$  species. The spectral features from the initial  $0.5\%\text{F}_2/\text{Ar}$  experiment shown in Fig. 7 will be considered in detail in turn, starting with the lowest energy ones.

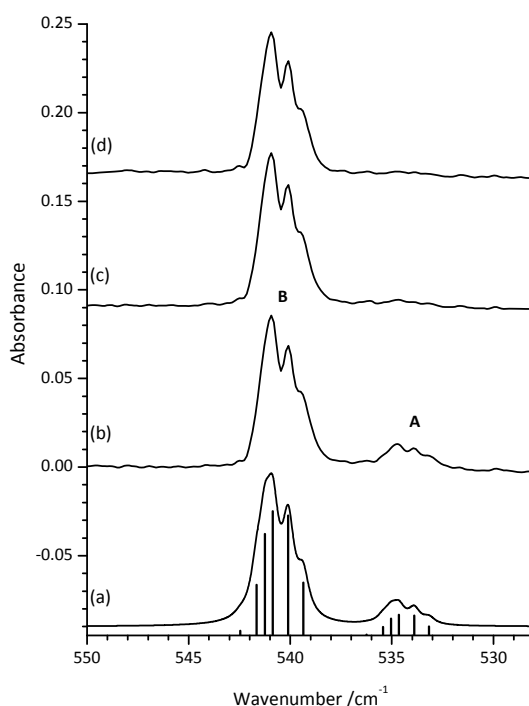


Figure 8. IR spectra of reaction products from thermally evaporated Pd atoms in a  $0.5\% \text{F}_2/\text{Ar}$  matrix

Fig. 8(b) shows in detail the bands at  $540\text{ cm}^{-1}$  (B) and  $534\text{ cm}^{-1}$  (A) (in Fig. 7) after deposition of Pd atoms into a  $0.5\% \text{F}_2/\text{Ar}$

(a) SVFF calculated spectrum for a PdF unit ( $^{108}\text{Pd } 540.1\text{ cm}^{-1}$ ,  $^{108}\text{Pd } 533.9\text{ cm}^{-1}$ ,  $0.7\text{ cm}^{-1}$  bandwidth), (b) on deposition, (c) after broad band photolysis, (d) after annealing to 25 K.

matrix. After broad band photolysis (Fig. 8(c)) there was a marked decrease in the intensity of the  $534\text{ cm}^{-1}$  (A) peaks, and subsequent annealing to 25 K (Fig. 8(d)) removed them altogether. It will be recalled from Fig. 1 that the Pd isotope pattern associated with PdF is very different from  $\text{PdF}_2$ . Although the Pd isotope structure on both of the features in Fig. 8 is not fully resolved, the SVFF calculations (using values of  $540.1$  and  $533.9\text{ cm}^{-1}$  for the  $^{108}\text{Pd}$  components of the two bands, see Table 3) in Fig. 8(a) confirm that both are consistent with a “PdF” unit rather than a “PdF<sub>2</sub>” unit.

In the thermal evaporation experiments there are three other sets of bands at  $692\text{ cm}^{-1}$  (E),  $624\text{ cm}^{-1}$  (D) and  $617\text{ cm}^{-1}$  (C) all of which display characteristic Pd isotopic structure.

The bands at  $630 - 600\text{ cm}^{-1}$  immediately after deposition of palladium atoms in a  $0.5\%F_2/Ar$  matrix are shown in Fig. 9

(f), and there is a difference in behaviour between these two sets of bands on broadband photolysis and annealing. The intensity of the higher energy set (D) centered at  $624\text{ cm}^{-1}$  reduced slightly on broadband photolysis (Fig. 9(g)), and then disappeared on annealing to  $25\text{ K}$  (Fig. 9(h)). In other experiments with  $0.5\% F_2/Ar$  matrices the higher energy multiplet at  $624\text{ cm}^{-1}$  (D) had greater relative intensity than the (C) set at

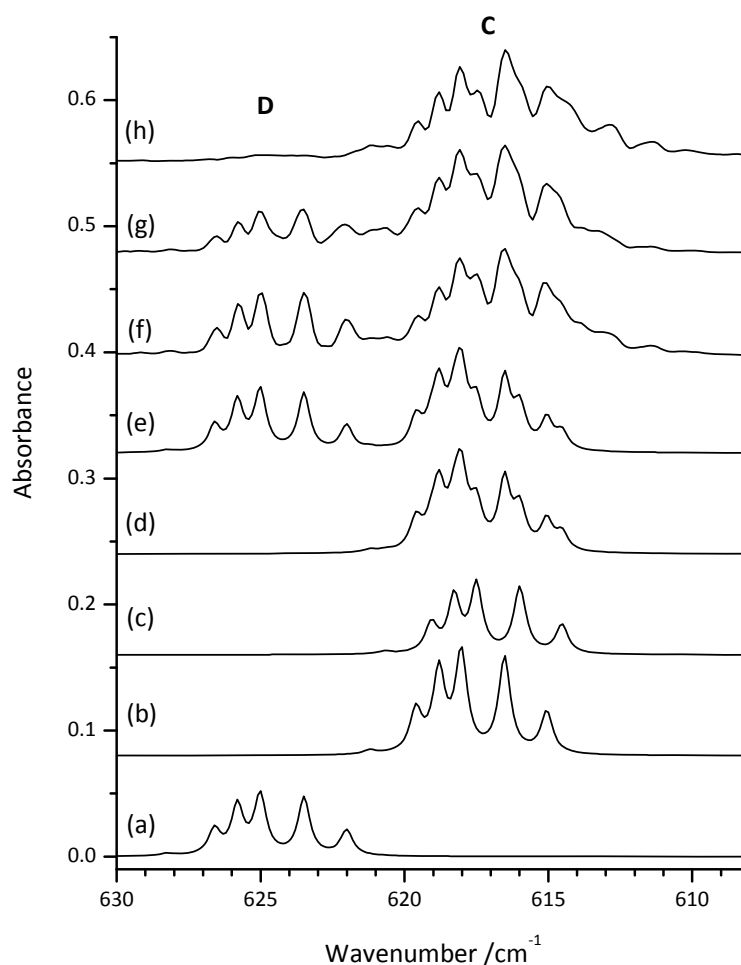


Figure 9. SVFF calculated spectra for a linear  $PdF_2$  unit (a)  $^{108}Pd$   $623.5\text{ cm}^{-1}$ , (b)  $^{108}Pd$   $616.5\text{ cm}^{-1}$ , (c)  $^{106}Pd$   $617.5\text{ cm}^{-1}$ , (d) sum of (b, c), (e) sum of (a, d). IR spectra of reaction products from thermally evaporated Pd atoms in a  $0.5\% F_2/Ar$  matrix (f) on deposition, (g) after broadband photolysis, (h) after annealing to  $25\text{ K}$ .

$617\text{ cm}^{-1}$  and could also be photobleached by prolonged photolysis. No other features in the  $\nu_{PdF}$  region have the same photolysis and annealing behaviour as these  $624\text{ cm}^{-1}$  bands. The SVFF calculations in Fig. 9(a) and Table 3 indicate that the Pd isotope pattern on the  $624\text{ cm}^{-1}$  feature is consistent with a linear “ $PdF_2$ ” unit (the  $^{108}Pd$  peak position of  $623.5\text{ cm}^{-1}$  is used as the starting

point for the calculations, because although it is not the most intense, it is clearly resolved). There is a slight reduction in the separation of the observed positions compared to the SVFF calculated values which could be taken as an indication of slight bending of the “PdF<sub>2</sub>”, or an increase in the effective mass of the palladium atom, but the measurements are at the limit of the experimental uncertainty. It should be noted that once deposition was complete, the 624 cm<sup>-1</sup> features never grew in intensity, and were only ever depleted by photolysis and annealing.

Within the set of (C) bands at 617 cm<sup>-1</sup>, there is a slight change in the relative intensity of the components on both photolysis and annealing (Fig. 9(f)-(h)) and this indicates that there are two Pd isotope patterns slightly offset from each other within this set of bands. The major component can be simulated with a linear “PdF<sub>2</sub>” unit with <sup>108</sup>Pd at 616.5 cm<sup>-1</sup> as shown in Fig. 9(b) and Table 3. The second set of bands consists of shoulders separated by about 0.5 cm<sup>-1</sup> from the main one. The peak at 617.5 cm<sup>-1</sup> belonging to this set was used to simulate an SVFF linear “PdF<sub>2</sub>” isotope pattern using both <sup>106</sup>Pd and <sup>108</sup>Pd as the starting point. The former (Fig. 9(c)) gave a very good fit when combined with the major component (Fig. 9(b)) as shown in Fig. 9(d). The overall SVFF simulation using the three calculations involving linear “PdF<sub>2</sub>” units is shown in Fig. 9(e), and the match to the experimental data in Fig. 9(f) is very good. To low energy of the main C peaks at 617 cm<sup>-1</sup> there are a set of weak peaks at 614.2, 612.7 and 611.4 cm<sup>-1</sup> indicative of Pd isotopic structure associated with a linear “PdF<sub>2</sub>” unit. These already weak features on deposition reduced on broadband photolysis, but grew on annealing to 25 K (Fig. 9(h)).

However, in a second experiment they grew on prolonged photolysis and then reduced on annealing. Given how weak they are they were not included in the SVFF final fit.

The only remaining peaks displaying Pd isotope structure in Fig. 6 and 7 are those labelled E at 692 cm<sup>-1</sup>. These are barely present on deposition (Fig. 10(a)), but grow on both photolysis (Fig. 10(b)) and annealing to 25 K (Fig. 10(c)). The SVFF simulation (Fig. 10(d) and Table 3) is consistent with a species containing a linear “PdF<sub>2</sub>” unit. As for the 617 cm<sup>-1</sup> features (C) there is evidence for shoulders indicating

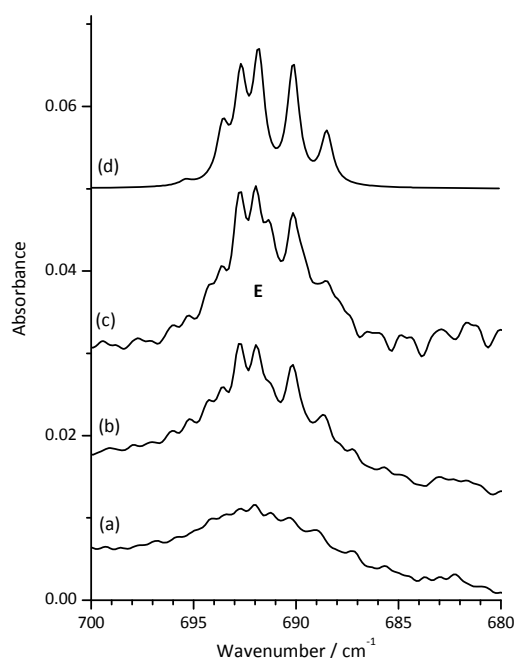


Figure 10. IR spectra of reaction products from thermally evaporated Pd atoms in a 0.5% F<sub>2</sub>/Ar matrix (a) on deposition, (b) after broad band photolysis, (c) after annealing to 25 K, (d) SVFF calculated spectrum for a linear PdF<sub>2</sub> unit with <sup>108</sup>Pd at 690.2 cm<sup>-1</sup>.

two species, but given the quality of the data they have not been simulated in this case.

Therefore, the peaks labelled **A** and **B** are consistent with “Pd-F” units, whilst those labelled **C**, **D**, **E** are consistent with linear “F-Pd-F” units. On the basis of both photolysis and annealing behaviour, all the peaks with Pd isotopic structure appear to be from distinct species.

With the aim of increasing the proportion of the higher fluorides, 10% F<sub>2</sub>/Ar matrices were also employed. However, broader bands were observed where it was impossible to identify any Pd isotopic structure. Given the number of bands that are expected in the  $\nu_{\text{Pd-F}}$  region from F<sub>2</sub> impurity interactions this is especially problematic.<sup>5</sup> A feature at 690 cm<sup>-1</sup> was more intense than the overlapping, poorly resolved features, at 615 and 607 cm<sup>-1</sup>, and no bands were observed at 540 or 534 cm<sup>-1</sup>, indicating that the higher wavenumber bands arise from higher oxidation state fluorides. On annealing to 25 K followed by broad band photolysis the 690 cm<sup>-1</sup> peak reduced in intensity and a shoulder grew in at 681 cm<sup>-1</sup>, which then grew on further annealing to 25 K. However, without Pd isotope patterns it is hard to assign these to PdF<sub>n</sub> species with any certainty.

## Laser ablation experiments

Fig. 11 shows the IR spectra obtained in Virginia after laser ablated Pd atoms were reacted with a 0.5% F<sub>2</sub>/Ar matrix. In addition to the [F<sub>3</sub>]<sup>-</sup> band at 510 cm<sup>-1</sup>,<sup>53</sup> a structured band with Pd isotopic structure (see insert) was observed at 617 cm<sup>-1</sup> together with another band at 540 cm<sup>-1</sup>, and these correspond to bands (C) and (B), respectively in the thermal evaporation experiments. After annealing to 20 K, a very weak feature at 692 cm<sup>-1</sup> was observed which decreased on photolysis with λ > 380 nm and full arc photolysis, but then re-appeared with increased intensity after annealing to 30 K. This corresponds to band (E) in the thermal evaporation experiments. In addition, annealing to 30 K resulted in the appearance of a new band (with Pd isotopic structure consistent with a linear “PdF<sub>2</sub>” unit) at 611 cm<sup>-1</sup>. These peaks grew further after annealing to 35 K, while the intensity of the peaks at 692, 617 and 540 cm<sup>-1</sup> all decreased. These new features are in a similar region to those observed in the thermal evaporation experiments to the low energy side of the 617 cm<sup>-1</sup> bands, but they are not at identical energy. Apart from the lack of the 624 cm<sup>-1</sup> bands (which are very photosensitive), these observations are in very good agreement with the thermal evaporation data.

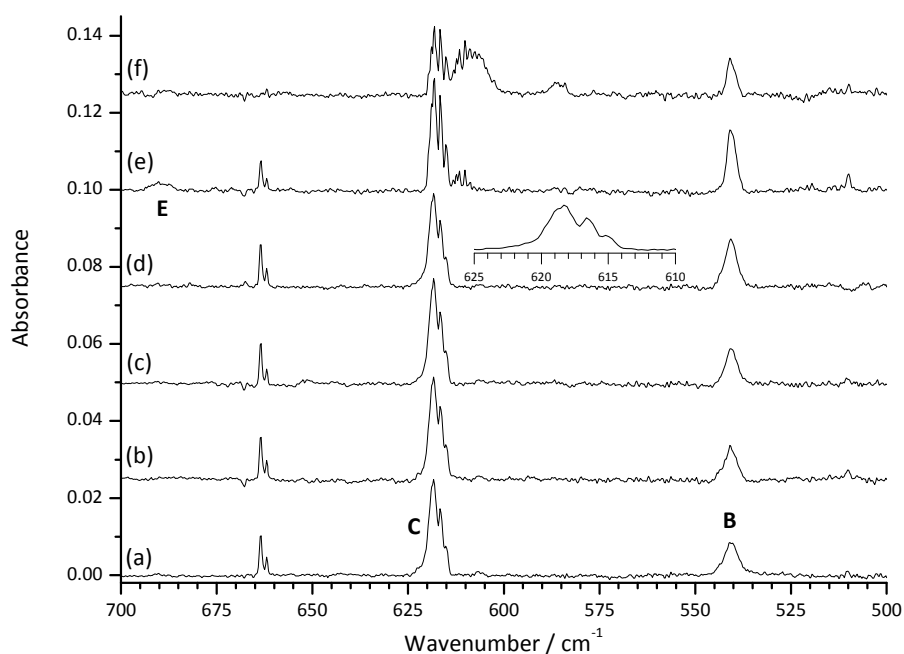


Figure 11. IR spectra of reaction products from laser-ablated Pd atoms in a 0.5% F<sub>2</sub>/Ar matrix (a) on deposition, (b) after annealing to 20 K, (c) after photolysis > 380 nm, (d) after full arc photolysis, (e) after annealing to 30 K, (f) after annealing to 35 K. (inset) Expansion of spectrum (d).

The results of the Pd laser ablation experiments carried out at Freiburg/Berlin with F<sub>2</sub> doped argon matrices were also very similar to those observed from the thermal evaporation experiments and the Virginia based laser ablation experiments, except that the [F<sub>3</sub>]<sup>-</sup> band at 510 cm<sup>-1</sup><sup>53</sup> was more intense relative to those of the PdF<sub>n</sub> features. In a 2% F<sub>2</sub>/Ar matrix (Fig. 12), bands with Pd isotopic structure were observed on deposition at 617 cm<sup>-1</sup> together with weaker features at 624 cm<sup>-1</sup> and these correspond to bands (C) and (D) in the thermal evaporation experiments. A weak feature, with poorly resolved Pd isotope structure was also observed at 540 cm<sup>-1</sup> in agreement with peak (B) in the thermal evaporation experiments. There is a weak peak at 657 cm<sup>-1</sup>, but its assignment is complicated by the presence of atmospheric CO<sub>2</sub> at 667 cm<sup>-1</sup>, and in the thermal evaporation experiments it was assigned to the HF-CO<sub>2</sub> complex.<sup>89</sup> On annealing to 25 K (Fig. 12(b)) the bands centered at 617 cm<sup>-1</sup> increased in intensity, with a subtle change in the structure, as also observed in the thermal evaporation experiments. On UV photolysis (Fig. 12(c)), the 624 cm<sup>-1</sup> bands disappeared, and whilst masked by the R branch structure of the bending mode of atmospheric CO<sub>2</sub>, a weak feature also grew in at 692 cm<sup>-1</sup>, corresponding to peak (E) in the thermal evaporation experiments. In other argon experiments this feature was more marked.

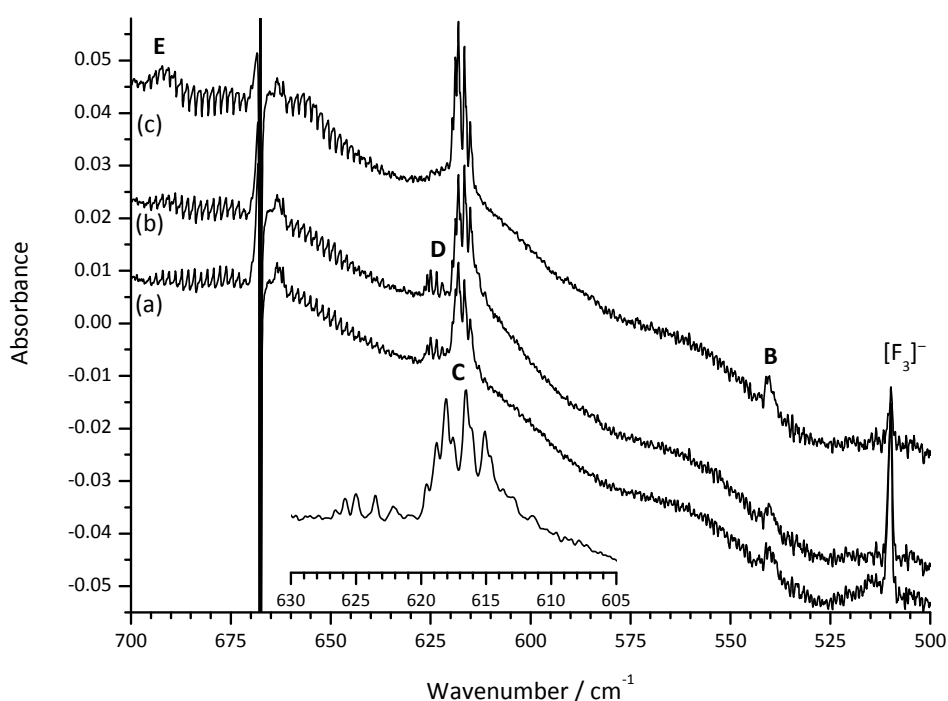


Figure 12. IR spectra of reaction products from laser-ablated Pd atoms in a 2% F<sub>2</sub>/Ar matrix (a) on deposition, (b) after annealing to 25 K, (c) after 15 min UV irradiation. (inset) Expansion of spectrum (b)

Therefore, there is a high level of agreement between the argon matrix data for the products generated by thermal evaporation and both laser ablation experiments.

When 0.5% F<sub>2</sub>/Ne matrices were employed in Berlin (Fig. 13), the only bands observed after deposition at 5 K to have Pd isotopic structure were at *ca.* 650 cm<sup>-1</sup>, and these persisted after annealing to 8 K and then 10 K. As in the argon matrix case, an intense band at 524.8 cm<sup>-1</sup> is assigned to [F<sub>3</sub>]<sup>-</sup>.<sup>52, 53</sup> In addition, a new band at 642 cm<sup>-1</sup> bearing Pd isotopic structure appeared on annealing to 8 K. This correlates with the argon matrix laser ablation experiments carried out in Virginia, where bands with Pd isotopic structure to slightly lower energy of the main ones at 617 cm<sup>-1</sup> grew on high temperature (35 K) annealing. The structured band in neon (Fig. 13) at 650 cm<sup>-1</sup> exhibited strongest resolved Pd isotopic peaks at 651.0, 649.3, 647.8 cm<sup>-1</sup>, and these are all shifted by 32.8 cm<sup>-1</sup> from the most intense features in the corresponding 2% F<sub>2</sub>/Ar spectrum (Fig. 12) (bands **(C)**) which showed strongest peaks at 618.2, 616.5, 615.0 cm<sup>-1</sup>. There were no features observed in these neon matrix data that corresponded to bands **(A)**, **(B)** or **(D)**. Although there was no clear evidence for the counterparts of the **E** bands at 692 cm<sup>-1</sup> in Ar, it should be remembered that photolysis was usually necessary to observe them, especially at this level of F<sub>2</sub> dilution. However, in separate Ne matrix experiments a weak band was observed at 685 cm<sup>-1</sup> after annealing to 11.5 K, and after photolysis this increased in intensity at the expense of the 650 cm<sup>-1</sup> bands.

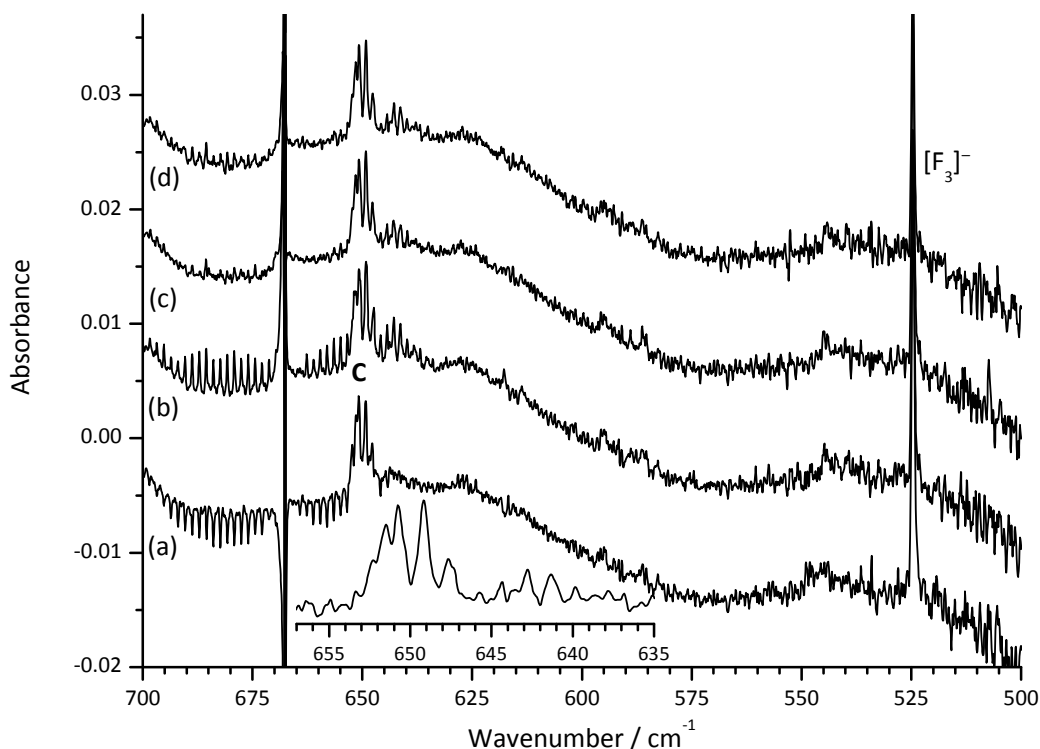


Figure 13. IR spectra of reaction products from laser-ablated Pd atoms in a 0.5% F<sub>2</sub>/Ne matrix (a) on deposition, (b) after annealing to 8 K, (c) after annealing to 8 K for 1 min, (d) after annealing to 10K. (inset) Expansion of spectrum (d).

When neat F<sub>2</sub> was used as a matrix gas in the Berlin laser ablation experiments (Fig. 14), the only bands with clear Pd isotopic structure were observed at 614 cm<sup>-1</sup>, which sharpened on annealing to 25 K, decreased on 365 nm photolysis and then again on annealing to 30 K. The band at 586 cm<sup>-1</sup> is due to OOF.<sup>90</sup> In addition, there is a band at 690 cm<sup>-1</sup> which although masked by the atmospheric CO<sub>2</sub> features does correspond to the set of bands labelled (E) in the argon matrix thermal evaporation experiments. There is no evidence for either of the sets of peaks labelled **A** or **B** confirming that these belong to lower oxidation state species. Published work on neat halogen matrices is fairly limited but it has been noted that the matrix shifts for argon and neat fluorine matrices are very similar.<sup>91</sup> A shift of 10 cm<sup>-1</sup> was observed for AuCl<sub>3</sub> between a 5% Cl<sub>2</sub>/Ar matrix and a neat Cl<sub>2</sub> matrix.<sup>49</sup> Therefore, the 614 cm<sup>-1</sup> bands in neat F<sub>2</sub> most likely to correspond to those at either 617 cm<sup>-1</sup> (**C**) or 624 cm<sup>-1</sup> (**D**) observed in the argon matrices. As the (**C**) bands were observed in all experiments it is most plausible to assign those in the neat F<sub>2</sub> experiments to the same carrier as **C** in the argon matrix experiments.

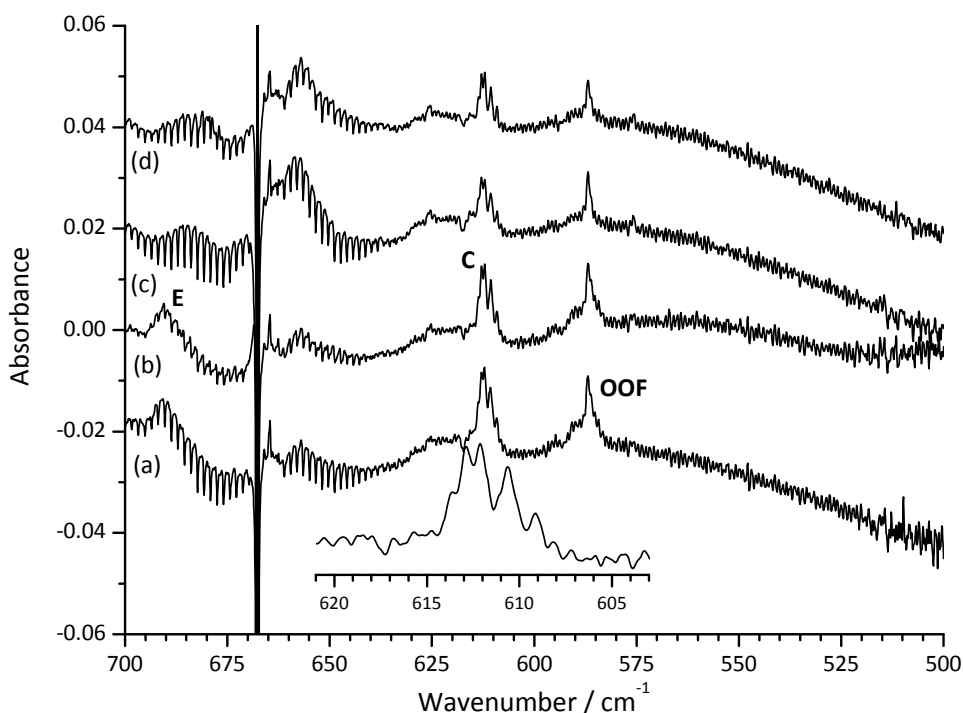


Figure 14. IR spectra of reaction products from laser-ablated Pd atoms in a neat  $F_2$  matrix (a) on deposition, (b) after annealing to 25 K, (c) after photolysis at 365 nm, (d) after annealing to 30 K. (inset) Expansion of spectrum (b).

## Discussion

The electronic absorption spectra indicate that under thermal evaporation conditions Pd atoms are being isolated in the argon matrices which go on and react with the fluorine, and that whilst in these experiments photolysis had little effect, there are at least two new species formed on annealing, that are dependent on the  $F_2$  concentration. The observed transition energies ( $38000 - 49000 \text{ cm}^{-1}$ ) are significantly greater than those calculated by David *et al.* using TDDFT for transitions to the lowest energy excited state in  $PdF_6$  ( $15560, 22760 \text{ cm}^{-1}$ ),<sup>11</sup> although there is a very broad and weak feature at lower energy observed only when the product bands are present.

Although it has been possible to identify the vibrational modes involving palladium, the lack of fluorine isotopic data makes unambiguous assignment of the vibrational modes to specific palladium fluorides very challenging. What is clear is that overall there is very good agreement between the three argon matrix experiments (thermal evaporation in Hull and laser ablation in Virginia and

Freiburg/Berlin), and also between the different matrix gases ( $F_2/Ar$ ,  $F_2/Ne$ ,  $F_2$ ). In summary, the features at  $692\text{ cm}^{-1}$  (**E**),  $617\text{ cm}^{-1}$  (**C**) and  $540\text{ cm}^{-1}$  (**B**) in the IR spectra of  $F_2$  doped Ar matrices containing Pd atoms were common to all thermal evaporation and laser ablation experiments. There are no counterparts of the  $534\text{ cm}^{-1}$  (**A**) band in either laser ablation experiment, and the  $624\text{ cm}^{-1}$  (**D**) features observed from thermal evaporation are observed in some of the Freiburg/Berlin laser ablation experiments, but not the Virginia ones. Neon was used as a matrix gas in the laser ablation experiments at Freiburg/Berlin and in these experiments only one band at  $650\text{ cm}^{-1}$  with clear Pd isotopic structure was observed on deposition, although a feature at  $685\text{ cm}^{-1}$  was detectable amongst the atmospheric  $CO_2$  features, together with a weak set of peaks to low wavenumber of the  $650\text{ cm}^{-1}$  feature that appeared at relatively high annealing temperatures. The neat  $F_2$  experiments were only carried out at Berlin, and as with the Freiburg/Berlin neon matrix experiments only yielded one set of bands with clear Pd isotopic structure, but there was evidence for a peak at  $690\text{ cm}^{-1}$  amongst the atmospheric  $CO_2$  peaks. The absence of the bands labelled **D** in some of the laser ablation experiments is most likely due to the effects of the intense radiation field associated with ablation, as these bands were very sensitive to both photolysis and annealing, and were never observed to increase in intensity once deposition was complete. Therefore, the absence of some bands may be as a result of photobleaching of photosensitive species.

The changes in the relative intensity of the IR bands in the different  $F_2/Ar$  matrices imply that in general those at lower wavenumber are associated with lower coordination number/oxidation state palladium fluorides than those at higher wavenumber. The annealing and photolysis behaviour of the absorption bands in the thermal evaporation experiments of Pd atoms indicate that none of the IR bands with Pd isotope structure at  $692\text{ cm}^{-1}$  (**E**),  $624\text{ cm}^{-1}$  (**D**),  $617\text{ cm}^{-1}$  (**C**),  $540\text{ cm}^{-1}$  (**B**) and  $534\text{ cm}^{-1}$  (**A**) are from the same species. As there is no evidence for second bands with the same annealing and photolysis behaviour as any of these five, it is not easy to assign any of them to either  $PdF_3$  or  $PdF_5$ , but the expected weaker bands could be of too low intensity to be observed above the noise level, or hidden under another more intense feature. The palladium fluorides are predicted (at the relativistic DFT level) to have intense bands at  $534\text{ cm}^{-1}$  ( $PdF$ ),  $634\text{ cm}^{-1}$  ( $PdF_2$ ),  $648.0\text{ cm}^{-1}$  ( $PdF_5$  and  $PdF_6$ ),  $662\text{ cm}^{-1}$  ( $PdF_3$ ) and  $664\text{ cm}^{-1}$  ( $PdF_4$ ) with weaker features at  $565\text{ cm}^{-1}$  for  $PdF_3$  and  $633\text{ cm}^{-1}$  for  $PdF_5$ , respectively. It should be remembered that  $PdF_2$ <sup>36</sup> and  $PdF_4$ <sup>41, 42</sup> are well characterized solid state materials, but " $PdF_3$ " is mixed valent, and is best thought of as  $Pd(II)[Pd(IV)F_6]$ , with both palladium atoms are in an octahedral fluoride environment.<sup>37-40</sup>

The  $540\text{ cm}^{-1}$  peak (**B**) was common to both the laser ablation and thermal evaporation experiments using argon matrices, whilst the  $534\text{ cm}^{-1}$  peak (**A**) was only observed in the thermal evaporation

work and was readily removed by photolysis and annealing. The Pd isotope patterns on the 540 and 534  $\text{cm}^{-1}$  peaks (Fig. 8) are consistent with the assignment of these two peaks to PdF (or “PdF” units). The almost complete reduction in the intensity of the 534  $\text{cm}^{-1}$  band after broad band photolysis and its disappearance on annealing is not associated with a decrease in any of the other features, including the bands at 624  $\text{cm}^{-1}$ , therefore it cannot be assigned to a “PdF” unit in PdF<sub>3</sub> or PdF<sub>5</sub>. The calculated value for PdF is 531  $\text{cm}^{-1}$ <sup>45</sup> or 533.9  $\text{cm}^{-1}$  from this work. Therefore, these bands can be readily assigned to PdF. The most straight-forward assignment is for the 540  $\text{cm}^{-1}$  bands to PdF, and the 534  $\text{cm}^{-1}$  bands to PdF in a slightly different site which can be removed by photolysis and annealing. A possibility is that PdF is isolated in close proximity to an F atom or F<sub>2</sub> molecule with which it can readily react resulting in an increase in the peaks at 692  $\text{cm}^{-1}$  and possibly 617  $\text{cm}^{-1}$ . The observation of PdF on deposition of thermal Pd atoms with F<sub>2</sub> indicates that the Pd + F<sub>2</sub> → PdF + F reaction is spontaneous and that F atoms are therefore present in the matrix, in addition to F<sub>2</sub>. Similar evidence was also observed in the analogous Ti work.<sup>50</sup> In dilute F<sub>2</sub>/Ne matrices a corresponding weak band with poorly resolved palladium isotope structure was observed at 545  $\text{cm}^{-1}$ . In neat F<sub>2</sub> matrices there was no evidence for a peak belonging to PdF, as to be expected. This work represents the first spectroscopic characterization of molecular PdF.

In the 630-600  $\text{cm}^{-1}$  region of the argon matrix data there are four IR bands displaying Pd isotopic structure in the thermal evaporation data, one set at 624  $\text{cm}^{-1}$  a second overlapping pair at 617  $\text{cm}^{-1}$  and very weak set at 612  $\text{cm}^{-1}$ . The 617  $\text{cm}^{-1}$  bands are also in both of the laser ablation experiments, but the 624  $\text{cm}^{-1}$  bands are only present in the Freiburg/Berlin laser ablation work, and not the Virginia experiments. However, high temperature annealing in the Virginia experiments resulted in bands at 611  $\text{cm}^{-1}$ .

The 617  $\text{cm}^{-1}$  features were observed in all of the thermal and laser ablation experiments with argon matrices, and with Pd isotopic structure consistent with a linear “PdF<sub>2</sub>” unit it seems reasonable to assign them to PdF<sub>2</sub>, especially as the calculations indicate this has the lowest vibrational frequency apart from PdF. The second set of bands displaying Pd isotope structure overlapping these could be due to another species but as the separation between them is of the order of 0.5  $\text{cm}^{-1}$  a more reasonable assignment would be to a second site for PdF<sub>2</sub>. Whilst the two sets could feasibly arise from the two modes expected for either *D*<sub>2d</sub> or *D*<sub>2h</sub> distorted PdF<sub>4</sub>, the second site explanation is much more likely, especially as a similar situation was observed for linear TiF<sub>2</sub> in argon matrices, where two sites could also be modelled successfully.<sup>50</sup> As the 617  $\text{cm}^{-1}$  bands assigned to PdF<sub>2</sub> were present in all dilute F<sub>2</sub>/Ar matrices, it would seem sensible to assign the only bands observed with clear Pd isotopic structure in 0.5% F<sub>2</sub>/Ne matrices at 650  $\text{cm}^{-1}$  to PdF<sub>2</sub> as well. This is a relatively large

argon to neon matrix shift, which may be compared with the  $15\text{ cm}^{-1}$  shift observed for the matrix isolated  $[\text{F}_3]^-$  anion,<sup>53</sup> and  $22\text{ cm}^{-1}$  for  $\text{FeF}_2$ ,  $15.1\text{ cm}^{-1}$  for  $\text{FeF}_3$  and  $21.6\text{ cm}^{-1}$  for  $\text{FeF}_4$ .<sup>52</sup> The large matrix shift of  $32.8\text{ cm}^{-1}$  indicates that the Pd centre is vulnerable to interactions with the matrix atoms because it is not saturated with bound F atoms. In neat  $\text{F}_2$  matrices bands with Pd isotopic structure were observed at  $614\text{ cm}^{-1}$  and as  $\text{PdF}_2$  was observed in all the other experiments, it is reasonable to assign these features to  $\text{PdF}_2$  as well. These data represent the first spectroscopic characterization of molecular  $\text{PdF}_2$ .

There were weak peaks to lower wavenumber than the (C) peaks in both the thermal evaporation and laser ablation experiments after photolysis and annealing, but not at identical values or with identical behaviour. The  $611\text{ cm}^{-1}$  peaks observed after relatively high temperature annealing in the Virginia laser ablation experiments clearly have Pd isotopic structure consistent with a linear “ $\text{PdF}_2$ ” unit (Fig. 11), whereas this is less clear in the thermal evaporation data. These are most likely due to unidentified aggregation products formed on high temperature annealing.

The peaks at  $692\text{ cm}^{-1}$  in dilute  $\text{F}_2/\text{Ar}$  matrices are very weak after deposition, but grow on photolysis and annealing in both the thermal evaporation and laser ablation experiments, indicating that they are the result of species formed from reaction of Pd or  $\text{PdF}_n$  with either fluorine atoms or fluorine molecules. They are also relatively more intense in the matrices with a higher concentration of  $\text{F}_2$ . The Pd isotopic structure from the thermal evaporation experiments (Fig. 10) is consistent with a linear “ $\text{PdF}_2$ ” unit and there does not appear to be any other  $\nu_{\text{Pd-F}}$  bands that have the same photolysis and annealing behaviour. In neat  $\text{F}_2$  matrices corresponding features were observed at  $690\text{ cm}^{-1}$ , and in dilute Ne matrices at  $685\text{ cm}^{-1}$ . The relativistic DFT calculations indicate that  $\text{PdF}_4$  will have the highest energy  $\nu_{\text{Pd-F}}$  modes of the palladium fluorides, and our CC calculations on  $\text{PdF}_4$  and  $\text{PdF}_6$  (see ESI) also indicate that the IR active  $\nu_{\text{Pd-F}}$  modes of  $\text{PdF}_4$  will be higher than those of  $\text{PdF}_6$ . Therefore, on the basis that solid state  $\text{PdF}_4$  is well known;<sup>41, 42</sup> the concentration, annealing and photolysis behaviour of the peaks at  $692\text{ cm}^{-1}$  in argon matrices (and  $690\text{ cm}^{-1}$  in  $\text{F}_2$ , and  $685\text{ cm}^{-1}$  in  $\text{F}_2/\text{Ne}$ ) indicate that they can be assigned to  $\text{PdF}_4$ . From the experimental data it is not possible to tell whether this is strictly square planar ( $D_{4h}$ ), or slightly distorted ( $D_{2d}$  or  $D_{2h}$ ) but the possibility of shoulders might indicate a small distortion, although a site effect explanation would be just as reasonable. As for PdF and  $\text{PdF}_2$ , this represents the first characterization of molecular  $\text{PdF}_4$ .

This leaves the assignment of the peaks at  $624\text{ cm}^{-1}$  in dilute argon matrices. The Pd isotope pattern (Fig. 9) indicates the presence of linear (or near linear) “ $\text{PdF}_2$ ” units. The annealing and photolysis

behaviour indicates that they belong to a reactive/unstable species with the major beneficiary appearing to be the bands at 692 and 612  $\text{cm}^{-1}$ . Under no conditions were these bands seen to grow once deposition had finished, and their reduction on annealing implies thermal instability, suggesting either a gain or loss of F to form a more stable species. With the lack of fluorine isotopic data it is a real challenge to be able to assign these with certainty to  $\text{PdF}_6$ ,  $\text{PdF}_5$  or  $\text{PdF}_3$ .

The relativistic DFT calculations predict the IR active  $\nu_{\text{Pd-F}}$  mode of  $\text{PdF}_6$  to be 18  $\text{cm}^{-1}$  higher than in  $\text{PdF}_2$  and 15  $\text{cm}^{-1}$  lower than  $\text{PdF}_4$ , both of which would be reasonably consistent with an assignment of the 624  $\text{cm}^{-1}$  peaks to  $\text{PdF}_6$ . Neat  $\text{F}_2$  experiments would be expected to stabilize the highest palladium fluoride, but the only band with clear Pd isotopic structure observed was at 614  $\text{cm}^{-1}$ , which is best assigned to  $\text{PdF}_2$  in comparison with all the other data. There was also evidence for another peak in neat  $\text{F}_2$  matrices at 690  $\text{cm}^{-1}$  which has been assigned to  $\text{PdF}_4$ . If the peaks at 624  $\text{cm}^{-1}$  in argon matrices are assigned to  $\text{PdF}_6$  it is very hard to explain why these  $\text{PdF}_6$  features at 624  $\text{cm}^{-1}$  should be present in the matrix before  $\text{PdF}_4$  at 692  $\text{cm}^{-1}$ , and that the latter is only really formed after photolysis and annealing, as well as there being no evidence for the 624  $\text{cm}^{-1}$  bands in the neat  $\text{F}_2$  matrix (unless those at 614  $\text{cm}^{-1}$  assigned to  $\text{PdF}_2$  are instead due to  $\text{PdF}_6$ ). The IR active mode of  $\text{PtF}_6$  is at 705  $\text{cm}^{-1}$ ,<sup>32,33</sup> and for the nearest 4d/5d pair to Pd/Pt, the IR active modes are at 724  $\text{cm}^{-1}$  ( $\text{RhF}_6$ )<sup>92</sup> and 719  $\text{cm}^{-1}$  ( $\text{IrF}_6$ ).<sup>33</sup> On this basis, as well as a band at 711  $\text{cm}^{-1}$  being assigned previously to  $\text{PdF}_6$ ,<sup>27,28</sup> an alternative assignment is that the peaks at 692  $\text{cm}^{-1}$  could be due to  $\text{PdF}_6$  and those at 624  $\text{cm}^{-1}$  to  $\text{PdF}_4$ . However, this is not supported by both the DFT and CC calculations which indicate that  $\text{PdF}_4$  will have higher IR active  $\nu_{\text{Pd-F}}$  modes than  $\text{PdF}_6$ , and the expectation that  $\text{PdF}_4$  would be more stable than  $\text{PdF}_6$ . Therefore, there is little convincing evidence for  $\text{PdF}_6$  in any of these experiments, but it is not completely ruled out.

Another possibility is that with the 692  $\text{cm}^{-1}$  bands being assigned to  $\text{PdF}_4$ , the photolysis and annealing behaviour of those at 624  $\text{cm}^{-1}$  indicate that these could be assigned to  $\text{PdF}_3$ , and that the second, weaker (calculated relative intensity of 3:1), IR active mode is either too weak to be observed above the noise level, or is masked by other features in the spectrum. The SVFF calculations indicate that the “ $\text{PdF}_2$ ” unit might be slightly bent, or the effective mass of the palladium is slightly increased, both of which would be consistent with ‘T-shaped’  $\text{PdF}_3$ . However, the relativistic DFT calculations indicate that the most intense  $\nu_{\text{Pd-F}}$  IR active mode in  $\text{PdF}_3$  will overlap that of  $\text{PdF}_4$  *ca.* 30  $\text{cm}^{-1}$  higher than that for  $\text{PdF}_2$ , but experimentally these bands are much closer to the those of  $\text{PdF}_2$  rather than  $\text{PdF}_4$ . Whilst it is tempting to assign the 534  $\text{cm}^{-1}$  feature as the second IR active mode of  $\text{PdF}_3$ , all the evidence points to the 624 and 534  $\text{cm}^{-1}$  peaks being from different species. The photolysis and annealing behaviour of the bands at 612  $\text{cm}^{-1}$  are also different

to that of the  $624\text{ cm}^{-1}$  set, so these are not the second set of  $\text{PdF}_3$  (or  $\text{PdF}_5$ ) bands either. Therefore, whilst the assignment of the  $624\text{ cm}^{-1}$  peaks to  $\text{PdF}_3$  is indicated by the experimental observation of their formation on deposition and subsequent depletion by annealing and photolysis, it is not completely satisfactory as there is only one band observed in the IR spectrum, and its relative position with respect to the other  $\text{PdF}_n$  species is not that predicted by the calculations.

The calculated values for the IR active  $\nu_{\text{Pd-F}}$  modes in  $\text{PdF}_5$  are at  $648$  and  $633\text{ cm}^{-1}$ , with an intensity ratio of *ca.* 10:1, and whilst these are more compatible with the peaks at  $624\text{ cm}^{-1}$ , the calculations indicate that  $\text{PdF}_5$  is the least stable of the palladium fluorides and is unstable with respect to disproportionation to  $\text{PdF}_4$  and  $\text{PdF}_6$ . Whilst  $\text{PtF}_5$  is known,<sup>93, 94</sup> there do not appear to be any reputable reports for  $\text{PdF}_5$ .<sup>1</sup> It is hard to rationalize why  $\text{PdF}_5$  should be formed, but not  $\text{PdF}_3$  or even  $\text{PdF}_6$ . Therefore, it seems that assigning the  $624\text{ cm}^{-1}$  features to  $\text{PdF}_5$  is the least likely option.

Therefore, it is not possible to make an unambiguous assignment of the  $624\text{ cm}^{-1}$  peaks in argon matrices, with  $\text{PdF}_6$ ,  $\text{PdF}_3$  and  $\text{PdF}_5$  all being possibilities, but  $\text{PdF}_6$  and  $\text{PdF}_3$  are the most plausible. Whilst the calculations (in terms of the position of the vibrational frequencies) indicate that  $\text{PdF}_6$  is the most probable, the experimental observations of the  $624\text{ cm}^{-1}$  bands being more intense on deposition than those assigned to  $\text{PdF}_4$  at  $692\text{ cm}^{-1}$ , and also very susceptible to photolysis and annealing would indicate that assigning them to  $\text{PdF}_3$  is the more sensible option. What is clear is that the species giving rise to the  $624\text{ cm}^{-1}$  bands is very photosensitive and thermally unstable even at cryogenic temperatures.

## Conclusions

This work has shown that there is a high degree of consistency between the thermal evaporation and laser ablation experiments, but that the high photon flux associated with the latter may photobleach some products. There are a total of seven sets of IR active bands that display Pd isotope behaviour in the  $\nu_{\text{Pd-F}}$  region when Pd atoms (produced by thermal evaporation or laser ablation) are trapped in  $\text{F}_2$  doped Ar matrices. In analogous neon and neat  $\text{F}_2$  experiments only one band displayed clear Pd isotopic structure, but there was evidence for others when taken together with the argon data. This work has been able to assign absorptions at  $540\text{ cm}^{-1}$  and  $617\text{ cm}^{-1}$  in argon matrices with confidence to  $\text{PdF}$  and  $\text{PdF}_2$ , respectively. The peaks at  $534\text{ cm}^{-1}$  are also consistent with a Pd-F unit, but do not correlate with any other peaks, and are assigned to  $\text{PdF}$  in a different site. Likewise, there is also a site effect on the  $\text{PdF}_2$  bands at  $617\text{ cm}^{-1}$ . This leaves the sets of peaks at  $692$ ,  $624$  and  $612\text{ cm}^{-1}$  which contain linear “ $\text{PdF}_2$ ” units, and do not seem to have any other sets

of bands associated with them. Those at  $692\text{ cm}^{-1}$  have behaviour consistent with a higher fluoride than  $\text{PdF}_2$  and as the calculations suggest that  $\text{PdF}_4$  will have the highest  $\nu_{\text{Pd-F}}$  mode these have been assigned to  $\text{PdF}_4$ . This is supported by the relative stability of  $\text{PdF}_4$ . The Pd isotopic structure on the bands at  $624\text{ cm}^{-1}$  indicates the presence of linear or near linear “ $\text{PdF}_2$ ” units, the photolysis and annealing indicates that there are no other IR active modes above the noise level associated with them, and that they are photosensitive and thermally unstable on annealing, with the biggest beneficiary appearing to be the bands at  $692$  and  $612\text{ cm}^{-1}$ . This suggests that there is either a gain or loss of F to form a more stable species. From the data available the most plausible assignment is to either  $\text{PdF}_6$  or  $\text{PdF}_3$ , with the latter being the most reasonable based on the experimental evidence, but this is by no means unambiguous. Therefore, whilst there is no convincing evidence for  $\text{PdF}_6$ , this detailed study has provided experimental evidence for  $\text{PdF}$ ,  $\text{PdF}_2$  and  $\text{PdF}_4$  for the first time. The lack of  $\text{PdF}_6$  is perhaps not that surprising as it is known that  $\text{XeF}_2$  will oxidize  $\text{PtF}_4$  and “ $\text{PdF}_3$ ”, but will not oxidize  $\text{PdF}_4$ .<sup>39</sup>

### Supporting Information

A table of non-relativistic DFT and CCSD computational results from this work, together with literature values for  $\text{PdF}_n$  species.

### Acknowledgements

The EPSRC are thanked for a studentship to AVW, and The University of Hull for financial support for the Hull based experiments. The experiments in Virginia were supported by N.S.F. grant CHE03-52487. The Freiburg/Berlin work was supported by the Fonds der Chemischen Industrie and the DFG. We also thank Dr. T. Ludwig from the University of Freiburg for help with the palladium target.

Table 3. IR data for palladium atom F<sub>2</sub> reaction products in cryogenic matrices.

Thermal Evaporation			Laser Ablation						
Hull (0.5% F <sub>2</sub> /Ar)			Virginia 0.5% F <sub>2</sub> /Ar	Freiburg Berlin 2% F <sub>2</sub> /Ar	Freiburg Berlin 0.5% F <sub>2</sub> /Ne	Berlin F <sub>2</sub>			
Observed	SVFF	Calculated <sup>†</sup>	Assignment	Observed	Observed	Observed	Observed		
<b>A</b>		536.2	<sup>102</sup> PdF						
		535.4	<sup>104</sup> PdF						
		535.0	<sup>105</sup> PdF						
	534.7	534.7	<sup>106</sup> PdF						
	533.9	533.9*	<sup>108</sup> PdF						
	533.2	533.2	<sup>110</sup> PdF						
<b>B</b>	Observed	SVFF	Calculated <sup>†</sup>						
			542.5	<sup>102</sup> PdF					
			541.7	<sup>104</sup> PdF					
			541.3	<sup>105</sup> PdF					
	540.9	540.9	<sup>106</sup> PdF						
	540.1	540.1*	<sup>108</sup> PdF						
539.4	539.4	<sup>110</sup> PdF							
<b>C</b>	Observed	SVFF	Calculated <sup>‡</sup>	Assignment	Observed	Observed	Observed	Observed	
			Site A	Site B					
			621.2		<sup>102</sup> PdF <sub>2</sub>				
	619.5	619.6		620.7	<sup>104</sup> PdF <sub>2</sub>	619.8		613.6	
				619.1	<sup>105</sup> PdF <sub>2</sub>				
	618.8	618.8		618.3	<sup>106</sup> PdF <sub>2</sub>	618.9	618.8	651.5	612.9
	618.1	618.0		617.5*	<sup>108</sup> PdF <sub>2</sub>	618.1	618.1	650.8	612.1
	617.5				<sup>110</sup> PdF <sub>2</sub>				
	616.5	616.5*				616.6	616.5	649.2	610.6
	616.0 (sh)			616.0					
	615.1	615.0				615.1	615.1	647.7	609.1
614.6 (sh)			614.5						
<b>D</b>	Observed	SVFF	Calculated <sup>‡</sup>	Assignment					
	628.1	628.3		<sup>102</sup> PdF <sub>3</sub> / <sup>102</sup> PdF <sub>6</sub>					
	626.5	626.6		<sup>104</sup> PdF <sub>3</sub> / <sup>104</sup> PdF <sub>6</sub>					
	625.7	625.8		<sup>105</sup> PdF <sub>3</sub> / <sup>105</sup> PdF <sub>6</sub>					
	625.0	625.0		<sup>106</sup> PdF <sub>3</sub> / <sup>106</sup> PdF <sub>6</sub>					
	623.5	623.5*		<sup>108</sup> PdF <sub>3</sub> / <sup>108</sup> PdF <sub>6</sub>					
622.0	622.0		<sup>110</sup> PdF <sub>3</sub> / <sup>110</sup> PdF <sub>6</sub>						
<b>E</b>	Observed	SVFF	Calculated <sup>‡</sup>	Assignment					
			695.5	<sup>102</sup> PdF <sub>4</sub>					
	693.6	693.6		<sup>104</sup> PdF <sub>4</sub>					
	692.7	692.8		<sup>105</sup> PdF <sub>4</sub>					
	691.9	691.9		<sup>106</sup> PdF <sub>4</sub>					
	690.2	690.2*		<sup>108</sup> PdF <sub>4</sub>					
688.5	688.6		<sup>110</sup> PdF <sub>4</sub>						

<sup>†</sup> assuming a linear "PdF" unit; <sup>‡</sup> assuming a linear "PdF<sub>2</sub>" unit, \*used to calculate other values

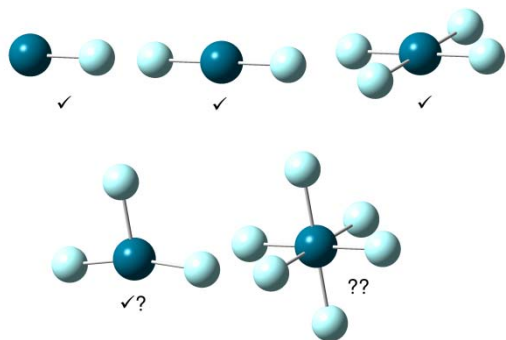
## References

- (1) Riedel, S.; Kaupp, M., *Coord. Chem. Rev.* **2009**, *253*, 606-624.
- (2) Seppelt, K., *Chem. Rev.* **2015**, *115*, 1296-1306.
- (3) Wang, X. F.; Andrews, L.; Riedel, S.; Kaupp, M., *Angew. Chem. Int. Ed.* **2007**, *46*, 8371-8375.
- (4) Hrobárik, P.; Kaupp, M.; Riedel, S., *Angew. Chem. Int. Ed.* **2008**, *47*, 8631-8633.
- (5) Rooms, J. F.; Wilson, A. V.; Harvey, I.; Bridgeman, A. J.; Young, N. A., *Phys. Chem. Chem. Phys.* **2008**, *10*, 4594-4605.
- (6) Andrews, L.; Wang, X. F.; Gong, Y.; Schlöder, T.; Riedel, S.; Franger, M. J., *Angew. Chem. Int. Ed.* **2012**, *51*, 8235-8238.
- (7) Drews, T.; Supel, J.; Hagenbach, A.; Seppelt, K., *Inorg. Chem.* **2006**, *45*, 3782-3788.
- (8) Molski, M. J.; Seppelt, K., *Dalton Trans.* **2009**, 3379-3383.
- (9) Vogt, T.; Fitch, A. N.; Cockcroft, J. K., *Science* **1994**, *263*, 1265-1267.
- (10) Aullón, G.; Alvarez, S., *Inorg. Chem.* **2007**, *46*, 2700-2703.
- (11) David, J.; Fuentealba, P.; Restrepo, A., *Chem. Phys. Lett.* **2008**, *457*, 42-44.
- (12) Craciun, R.; Long, R. T.; Dixon, D. A.; Christe, K. O., *J. Phys. Chem. A* **2010**, *114*, 7571-7582.
- (13) Siddiqui, S. A.; Bouarissa, N., *Solid State Sci.* **2013**, *15*, 60-65.
- (14) Riedel, S.; Renz, M.; Kaupp, M., *Inorg. Chem.* **2007**, *46*, 5734-5738.
- (15) Riedel, S.; Kaupp, M., *Angew. Chem. Int. Ed.* **2006**, *45*, 3708-3711.
- (16) Riedel, S.; Kaupp, M., *Inorg. Chem.* **2006**, *45*, 10497-10502.
- (17) Riedel, S.; Kaupp, M., *Inorg. Chem.* **2006**, *45*, 1228-1234.
- (18) Timakov, A. A.; Prusakov, V. N.; Drobyshevskii, I. V., *Dokl. Akad. Nauk SSSR* **1986**, *291*, 125-128.
- (19) Ostropikov, V. V.; Rakov, E. G., *Izv. Vyssh. Uchebn. Zaved., Khim. Khim. Tekhnol.* **1989**, *32*, 3-17.
- (20) Wesendrup, R.; Schwerdtfeger, P., *Inorg. Chem.* **2001**, *40*, 3351-3354.
- (21) Riedel, S., *J. Fluorine Chem.* **2007**, *128*, 938-942.
- (22) Gong, Y.; Zhou, M. F.; Andrews, L.; Schlöder, T.; Riedel, S., *Theor. Chem. Acc.* **2011**, *129*, 667-676.
- (23) Gong, Y.; Zhou, M. F.; Kaupp, M.; Riedel, S., *Angew. Chem. Int. Ed.* **2009**, *48*, 7879-7883.
- (24) Himmel, D.; Knapp, C.; Patzschke, M.; Riedel, S., *ChemPhysChem* **2010**, *11*, 865-869.
- (25) Wang, G. J.; Zhou, M. F.; Goettel, J. T.; Schrobilgen, G. J.; Su, J.; Li, J.; Schlöder, T.; Riedel, S., *Nature* **2014**, *514*, 475-477.
- (26) Pyykkö, P.; Xu, W. H., *Angew. Chem. Int. Ed.* **2015**, *54*, 1080-1081.
- (27) Timakov, A. A.; Prusakov, V. N.; Drobyshevskii, Y. V., *Zh. Neorg. Khim.* **1982**, *27*, 3007-3009.
- (28) Timakov, A. A.; Prusakov, V. N.; Drobyshevskii, Y. V., *Russ. J. Inorg. Chem.* **1982**, *27*, 1704-1706.
- (29) Shorafa, H.; Seppelt, K., *Inorg. Chem.* **2006**, *45*, 7929-7934.
- (30) Bartlett, N., *J. Fluorine Chem.* **2006**, *127*, 1285-1288.
- (31) Žemva, B.; Bartlett, N., *J. Fluorine Chem.* **2006**, *127*, 1463-1466.
- (32) Claassen, H. H.; Goodman, G. L.; Holloway, J. H.; Selig, H., *J. Chem. Phys.* **1970**, *53*, 341-348.
- (33) Holloway, J. H.; Stanger, G.; Hope, E. G.; Levason, W.; Ogden, J. S., *J. Chem. Soc., Dalton Trans.* **1988**, 1341-1345.
- (34) Bartlett, N., *Proc. Chem. Soc.* **1962**, 218.
- (35) Graham, L.; Graudejus, O.; Jha, N. K.; Bartlett, N., *Coord. Chem. Rev.* **2000**, *197*, 321-334.
- (36) Bartlett, N.; Maitland, R., *Acta Cryst.* **1958**, *11*, 747-748.
- (37) Bartlett, N.; Rao, P. R., *Proc. Chem. Soc.* **1964**, 393-394.
- (38) Tressaud, A.; Wintenberger, M.; Bartlett, N.; Hagenmuller, P., *C. R. Acad. Sci. Ser. C Paris* **1976**, *282*, 1069-1072.
- (39) Bartlett, N.; Žemva, B.; Graham, L., *J. Fluorine Chem.* **1976**, *7*, 301-320.
- (40) Hector, A. L.; Levason, W.; Weller, M. T.; Hope, E. G., *J. Fluorine Chem.* **1997**, *84*, 161-165.

- (41) Rao, P. R.; Tressaud, A.; Bartlett, N., *J. Inorg. Nucl. Chem.* **1976**, *28, Suppl. 1*, 23-28.
- (42) Wright, A. F.; Fender, B. E. F.; Bartlett, N.; Leary, K., *Inorg. Chem.* **1978**, *17*, 748-749.
- (43) Siegbahn, P. E. M., *Theor. Chim. Acta* **1993**, *86*, 219-228.
- (44) Siegbahn, P. E. M., *Theor. Chim. Acta* **1994**, *87*, 441-452.
- (45) Cheng, L.; Wang, M. Y.; Wu, Z. J.; Su, Z. M., *J. Comput. Chem.* **2007**, *28*, 2190-2202.
- (46) Cirera, J.; Ruiz, E.; Alvarez, S., *Inorg. Chem.* **2008**, *47*, 2871-2889.
- (47) Schlöder, T.; Riedel, S., 9.08 - Extreme Oxidation States of Transition Metals. In *Comprehensive Inorganic Chemistry II (Second Edition)*, Poeppelemeier, J. R., Ed. Elsevier: Amsterdam, 2013; pp 227-243.
- (48) Bridgeman, A. J.; Cavigliasso, G.; Harris, N.; Young, N. A., *Chem. Phys. Lett.* **2002**, *351*, 319-326.
- (49) Blackmore, I. J.; Bridgeman, A. J.; Harris, N.; Holdaway, M. A.; Rooms, J. F.; Thompson, E. L.; Young, N. A., *Angew. Chem. Int. Ed.* **2005**, *44*, 6746-6750.
- (50) Wilson, A. V.; Roberts, A. J.; Young, N. A., *Angew. Chem. Int. Ed.* **2008**, *47*, 1774-1776.
- (51) Andrews, L., *Chem. Soc. Rev.* **2004**, *33*, 123-132.
- (52) Schlöder, T.; Vent-Schmidt, T.; Riedel, S., *Angew. Chem. Int. Ed.* **2012**, *51*, 12063-12067.
- (53) Riedel, S.; Köchner, T.; Wang, X. F.; Andrews, L., *Inorg. Chem.* **2010**, *49*, 7156-7164.
- (54) Beattie, I. R.; Cheetham, N.; Gardner, M.; Rogers, D. E., *J. Chem. Soc. A* **1971**, 2240-2245.
- (55) te Velde, G.; Bickelhaupt, F. M.; Baerends, E. J.; Fonseca Guerra, C.; van Gisbergen, S. J. A.; Snijders, J. G.; Ziegler, T., *J. Comput. Chem.* **2001**, *22*, 931-967.
- (56) Fonseca Guerra, C.; Snijders, J. G.; te Velde, G.; Baerends, E. J., *Theor. Chem. Acc.* **1998**, *99*, 391-403.
- (57) *ADF2010. 2010*, SCM, Theoretical Chemistry, Vrije Universiteit, Amsterdam, The Netherlands, <http://www.scm.com>: 2010.
- (58) Becke, A. D., *Phys. Rev. A* **1988**, *38*, 3098-3100.
- (59) Perdew, J. P., *Phys. Rev. B* **1986**, *33*, 8822-8824.
- (60) Perdew, J. P., *Phys. Rev. B* **1986**, *34*, 7406-7406.
- (61) van Lenthe, E.; Ehlers, A.; Baerends, E. J., *J. Chem. Phys.* **1999**, *110*, 8943-8953.
- (62) Frisch, M. J.; Trucks, G. W.; Schlegel, H. B.; G. E. Scuseria; M. A. Robb, J. R. C., G. Scalmani, V. Barone, B. Mennucci, ; G. A. Petersson, H. N., M. Caricato, X. Li, H. P. Hratchian, ; A. F. Izmaylov, J. B., G. Zheng, J. L. Sonnenberg, M. Hada, ; M. Ehara, K. T., R. Fukuda, J. Hasegawa, M. Ishida, T. Nakajima, ; Y. Honda, O. K., H. Nakai, T. Vreven, J. A. Montgomery, Jr., ; J. E. Peralta, F. O., M. Bearpark, J. J. Heyd, E. Brothers, ; K. N. Kudin, V. N. S., T. Keith, R. Kobayashi, J. Normand, ; K. Raghavachari, A. R., J. C. Burant, S. S. Iyengar, J. Tomasi, ; M. Cossi, N. R., J. M. Millam, M. Klene, J. E. Knox, J. B. Cross, ; V. Bakken, C. A., J. Jaramillo, R. Gomperts, R. E. Stratmann, ; O. Yazyev, A. J. A., R. Cammi, C. Pomelli, J. W. Ochterski, ; R. L. Martin, K. M., V. G. Zakrzewski, G. A. Voth, ; P. Salvador, J. J. D., S. Dapprich, A. D. Daniels, ; O. Farkas, J. B. F., J. V. Ortiz, J. Cioslowski, ; Fox, D. J. *Gaussian 09, Revision B.01*, Wallingford CT, 2010.
- (63) *CFOUR, a quantum chemical program package written by J.F. Stanton, J. Gauss, M.E. Harding, P.G. Szalay, with contributions from A.A. Auer, R.J. Bartlett, U. Benedikt, C. Berger, D.E. Bernholdt, Y.J. Bomble, L. Cheng, O. Christiansen, M. Heckert, O. Heun, C. Huber, T.-C. Jagau, D. Jonsson, J. Jusélius, K. Klein, W.J. Lauderdale, F. Lipparini, D.A. Matthews, T. Metzroth, L.A. Mück, D.P. O'Neill, D.R. Price, E. Prochnow, C. Puzzarini, K. Ruud, F. Schiffmann, W. Schwalbach, C. Simmons, S. Stopkowicz, A. Tajti, J. Vázquez, F. Wang, J.D. Watts and the integral packages MOLECULE (J. Almlöf and P.R. Taylor), PROPS (P.R. Taylor), ABACUS (T. Helgaker, H.J. Aa. Jensen, P. Jørgensen, and J. Olsen), and ECP routines by A. V. Mitin and C. van Wüllen. .*
- (64) Peterson, K. A.; Figgen, D.; Dolg, M.; Stoll, H., *J. Chem. Phys.* **2007**, *126*, 124101.
- (65) Schwerdtfeger, P.; McFeaters, J. S.; Moore, J. J.; McPherson, D. M.; Cooney, R. P.; Bowmaker, G. A.; Dolg, M.; Andrae, D., *Langmuir* **1991**, *7*, 116-125.
- (66) Alipour, M.; Mohajeri, A., *Mol. Phys.* **2011**, *109*, 1439-1452.
- (67) Mohajeri, A.; Alipour, M., *J. Comput. Methods Sci. Eng.* **2011**, *11*, 301-311.

- (68) Chakraborty, D.; Chattaraj, P. K., *J. Phys. Chem. A* **2015**, *119*, 3064-3074.
- (69) David, J.; Guerra, D.; Restrepo, A., *Inorg. Chem.* **2011**, *50*, 1480-1483.
- (70) Alvarez-Thon, L.; David, J.; Arratia-Pérez, R.; Seppelt, K., *Phys. Rev. A* **2008**, *77*, 034502.
- (71) Forslund, L. E.; Kaltsoyannis, N., *New J. Chem.* **2003**, *27*, 1108-1114.
- (72) Alimi, R.; Gerber, R. B.; Apkarian, V. A., *J. Chem. Phys.* **1990**, *92*, 3551-3558.
- (73) Feld, J.; Kunttu, H.; Apkarian, V. A., *J. Chem. Phys.* **1990**, *93*, 1009-1020.
- (74) Misochko, E. Y.; Akimov, A. V.; Wight, C. A., *Chem. Phys. Lett.* **1997**, *274*, 23-28.
- (75) Mann, D. M.; Broida, H. P., *J. Chem. Phys.* **1971**, *55*, 84-94.
- (76) Klotzbücher, W. E.; Ozin, G. A., *Inorg. Chem.* **1976**, *15*, 292-295.
- (77) Klotzbücher, W. E.; Ozin, G. A., *Inorg. Chem.* **1980**, *19*, 3767-3776.
- (78) Schrittenlacher, W.; Rotermund, H. H.; Kolb, D. M., *J. Chem. Phys.* **1985**, *83*, 6145-6149.
- (79) Schrittenlacher, W.; Schroeder, W.; Rotermund, H. H.; Wiggerhauser, H.; Grinter, R.; Kolb, D. M., *J. Chem. Phys.* **1986**, *85*, 1348-1354.
- (80) Ozin, G. A.; Garcia-Prieto, J., *J. Phys. Chem.* **1988**, *92*, 318-324.
- (81) Ozin, G. A.; Garcia-Prieto, J., *J. Phys. Chem.* **1988**, *92*, 325-337.
- (82) Garcia-Prieto, J.; Novaro, O., *Rev. Mex. Fis.* **1997**, *43*, 130-158.
- (83) Souvi, S. M.; Tremblay, B.; Perchard, J. P.; Alikhani, M. E., *J. Chem. Phys.* **2009**, *130*, 074304.
- (84) Huber, H.; Kündig, E. P.; Moskovits, M.; Ozin, G. A., *J. Am. Chem. Soc.* **1973**, *95*, 332-344.
- (85) Klotzbücher, W. E.; Ozin, G. A., *J. Am. Chem. Soc.* **1975**, *97*, 2672-2675.
- (86) Ozin, G. A.; Klotzbücher, W. E., *J. Am. Chem. Soc.* **1975**, *97*, 3965-3974.
- (87) Huber, H.; Klotzbücher, W. E.; Ozin, G. A.; Vander Voet, A., *Can. J. Chem.* **1973**, *51*, 2722-2736.
- (88) Klotzbücher, W. E.; Ozin, G. A., *J. Am. Chem. Soc.* **1973**, *95*, 3790.
- (89) Andrews, L.; Johnson, G. L., *J. Chem. Phys.* **1982**, *76*, 2875-2880.
- (90) Jacox, M. E., *J. Mol. Spectrosc.* **1980**, *84*, 74-88.
- (91) Brosi, F.; Vent-Schmidt, T.; Kieninger, S.; Schlöder, T.; Beckers, H.; Riedel, S., *Chem. Eur. J.* **2015**, *21*, 16455-16462.
- (92) Brisdon, A. K.; Jones, P. J.; Levason, W.; Ogden, J. S.; Holloway, J. H.; Hope, E. G.; Stanger, G., *J. Chem. Soc., Dalton Trans.* **1990**, 715-718.
- (93) Müller, B. G.; Serafin, M., *Eur. J. Solid State Inorg. Chem.* **1992**, *29*, 625-633.
- (94) Hope, E. G., *Polyhedron* **1993**, *12*, 2977-2980.

## For Table of Contents Only



Matrix isolation IR data supported by calculations provides the first characterization of molecular PdF, PdF<sub>2</sub> and PdF<sub>4</sub>. An additional spectral feature is assigned to PdF<sub>3</sub>, but there is no unambiguous evidence for PdF<sub>6</sub>.